

AperTO - Archivio Istituzionale Open Access dell'Università di Torino

**The chronology of mysticete diversification (Mammalia, Cetacea, Mysticeti): Body size, morphological evolution and global change**

**This is the author's manuscript**

*Original Citation:*

*Availability:*

This version is available <http://hdl.handle.net/2318/1903252> since 2025-02-17T22:30:35Z

*Published version:*

DOI:10.1016/j.earscrev.2023.104373

*Terms of use:*

Open Access

Anyone can freely access the full text of works made available as "Open Access". Works made available under a Creative Commons license can be used according to the terms and conditions of said license. Use of all other works requires consent of the right holder (author or publisher) if not exempted from copyright protection by the applicable law.

(Article begins on next page)

1  
2  
3  
4  
5  
6  
7  
8  
9  
10  
11  
12  
13  
14  
15  
16  
17  
18  
19  
20  
21  
22  
23  
24  
25  
26  
27  
28  
29  
30  
31  
32  
33  
34  
35  
36  
37  
38  
39  
40  
41  
42  
43  
44  
45  
46  
47  
48  
49  
50  
51  
52  
53  
54  
55  
56  
57  
58  
59  
60  
61  
62  
63  
64  
65

**The chronology of mysticete diversification (Mammalia, Cetacea, Mysticeti): body size,  
morphological evolution and global change**

Bisconti M.<sup>1,2,\*</sup>, Pellegrino L.<sup>1</sup>, Carnevale G.<sup>1</sup>

<sup>1</sup>Dipartimento di Scienze della Terra, Università degli Studi di Torino, via Valperga Caluso 35,  
10100, Torino, Italy

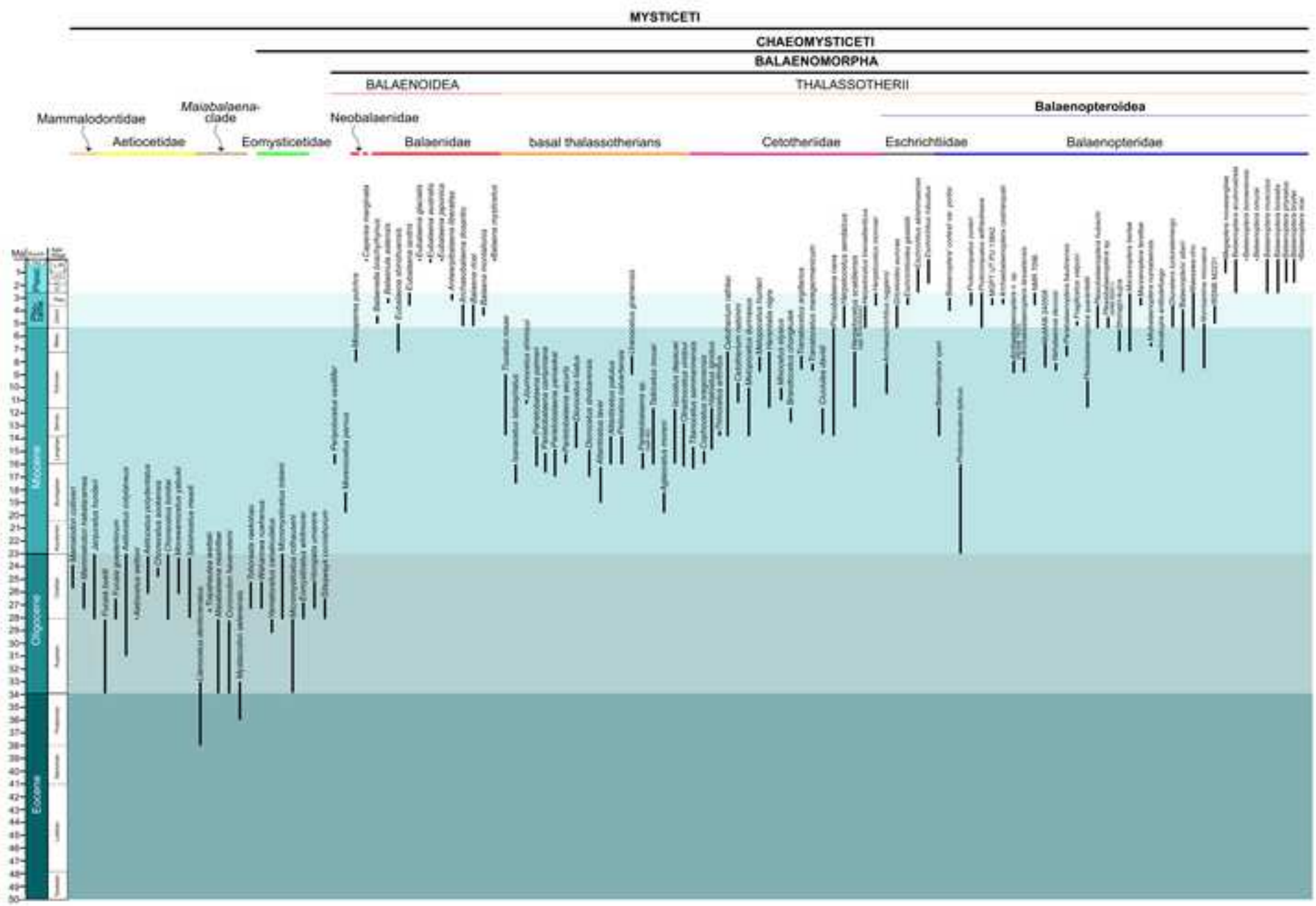
<sup>2</sup>San Diego Natural History Museum, 1788 El Prado, San Diego, 92292 California, USA

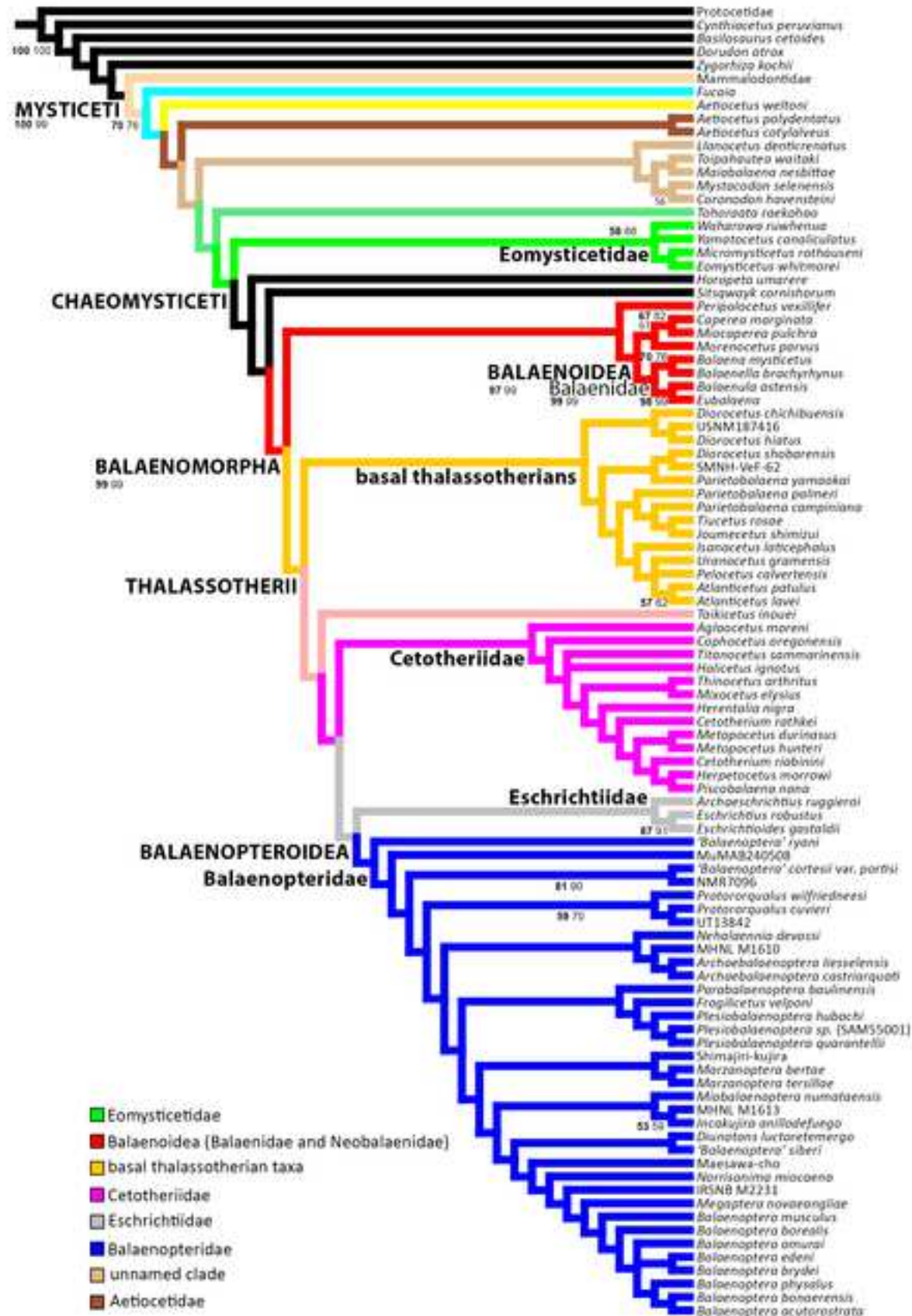
\*Corresponding author: Michelangelo Bisconti, e-mail: michelangelo.bisconti@unito.it

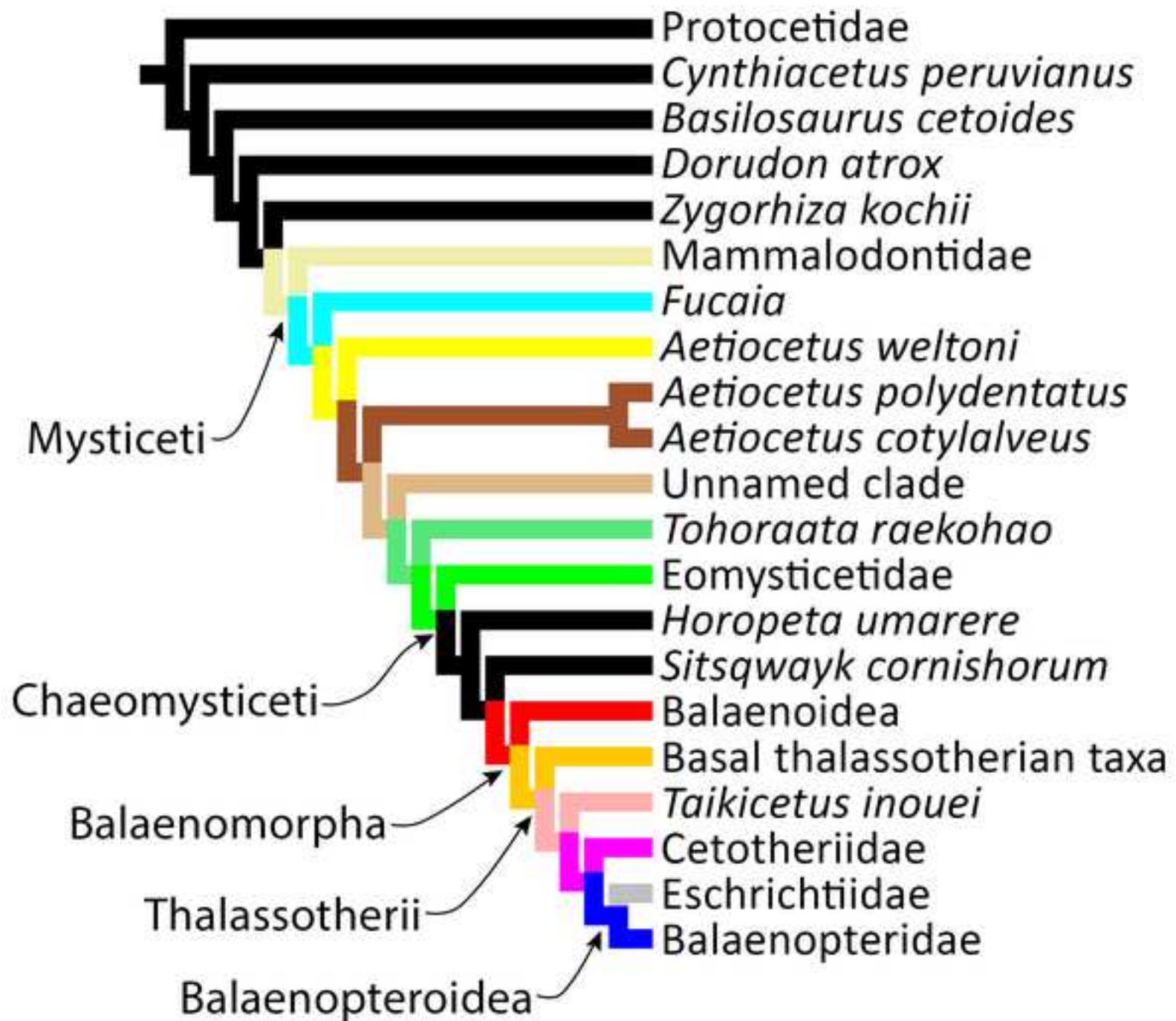
RUNNING TITLE: Chronology and evolution of mysticete clades

## Abstract

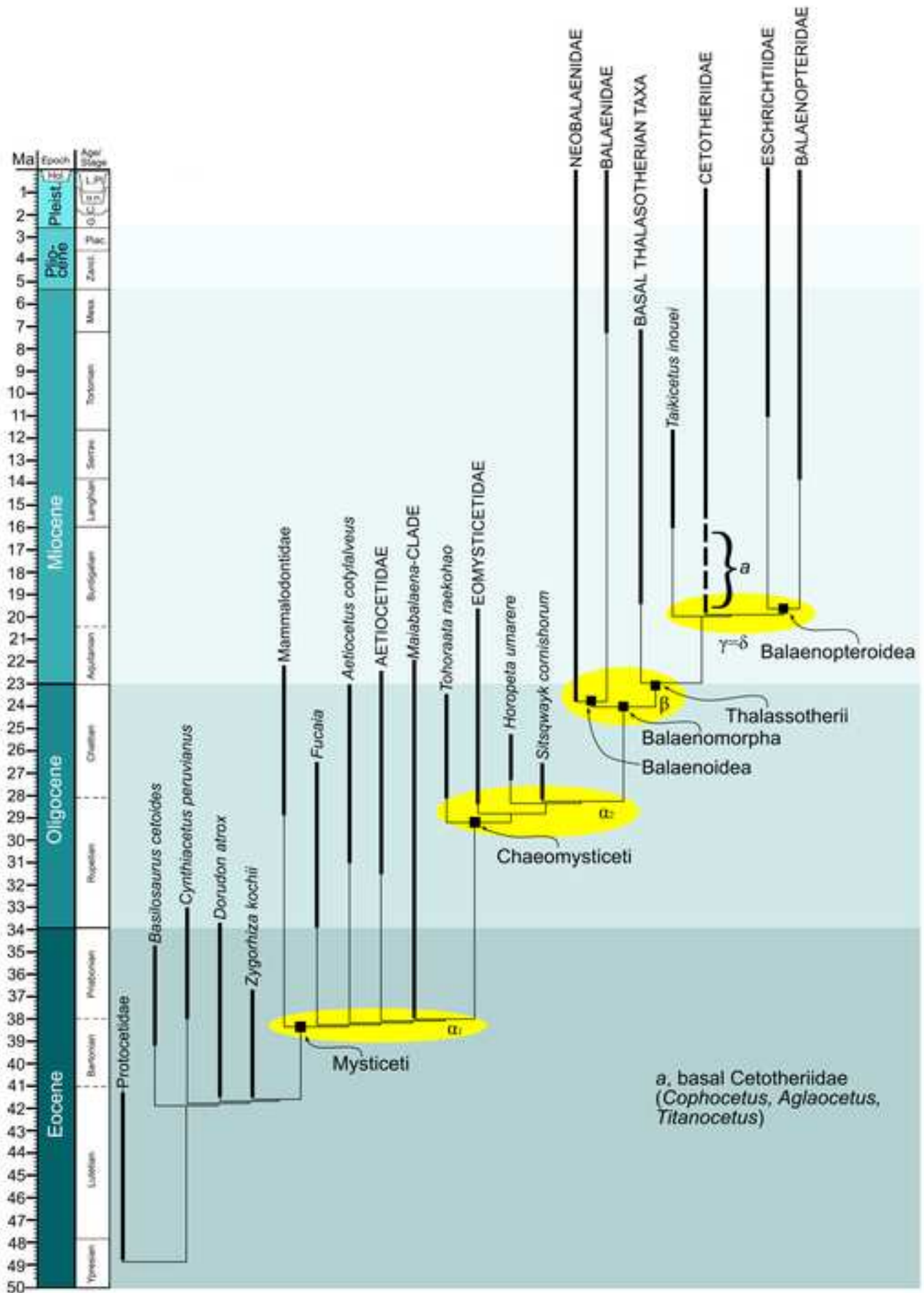
A comprehensive revision of the localities of discovery of fossil mysticetes is presented together with a highly inclusive phylogenetic analysis in order to provide the basis for a chronology of the main mysticete diversification events. The results suggest that the origin of Mysticeti (that include earlier toothed taxa together with today baleen-bearing cetaceans) occurred *c.* 38 Ma; the origin of Chaeomysticeti (that include only baleen-bearing cetaceans) occurred *c.* 28 Ma; the origin of Balaenomorpha (crown mysticetes) occurred *c.* 23.3 Ma. Additional chronological inferences are provided. Within this chronological framework, we analyzed diversity trends, origination and extinction patterns and body size evolution, and looked for eventual causal relationships between evolutionary processes, marine and terrestrial ecological turnovers and geodynamic events. We found five main diversification events corresponding to peaks in originations and, in a few cases, with the origin of different feeding strategies adopted by the different mysticete families. We found that different mechanisms are correlated to specific diversification events and these include changes in temperature and ocean circulation patterns, nutrient availability in the water column and diatom abundance and diversity. Resuming, no single mechanism explains all the diversification events occurred during mysticete evolution; rather, we found that each diversification event was correlated to different combinations of biotic and abiotic factors, suggesting that this group experienced major adaptation process to the changing paleoenvironments in the last 38 Ma.

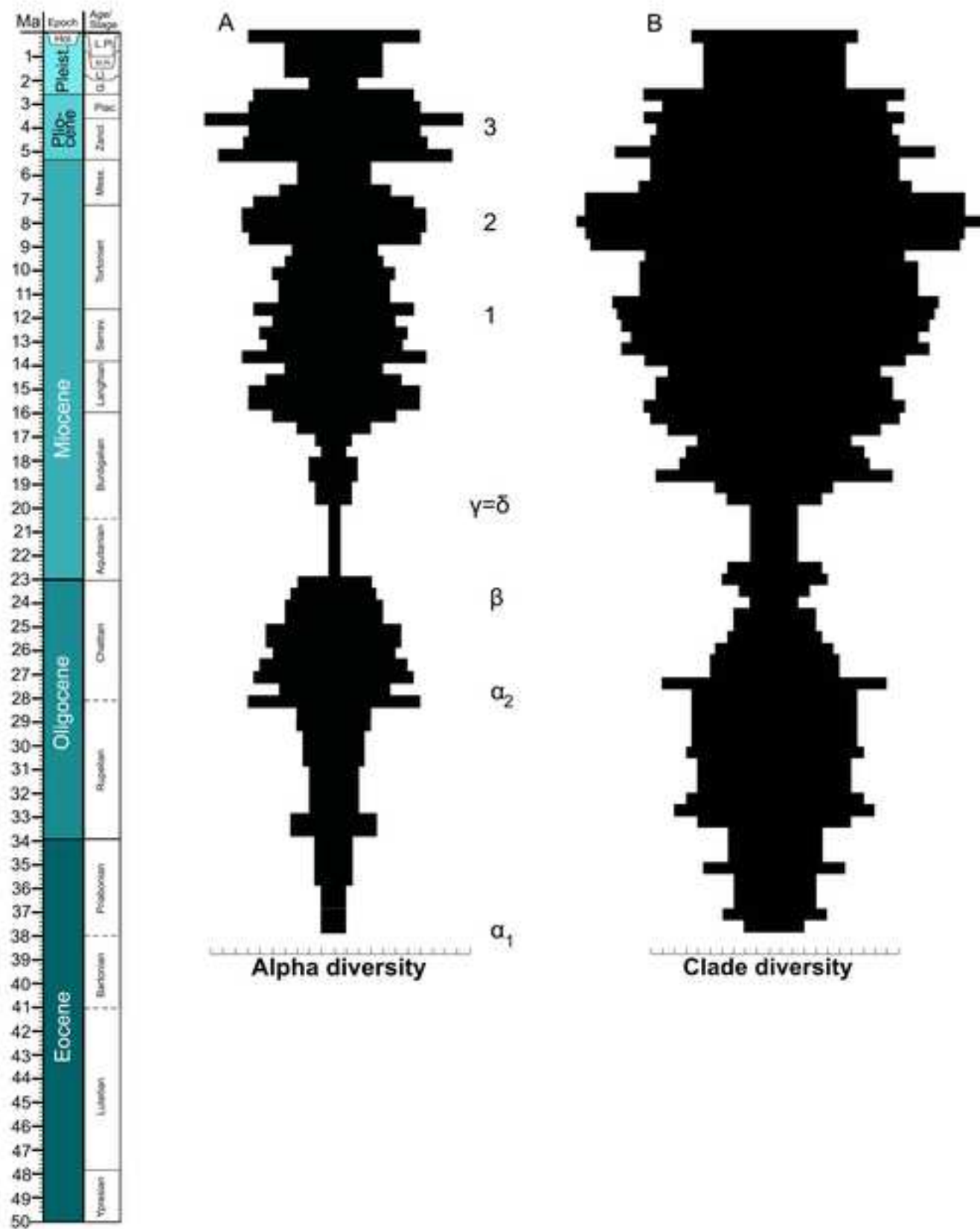




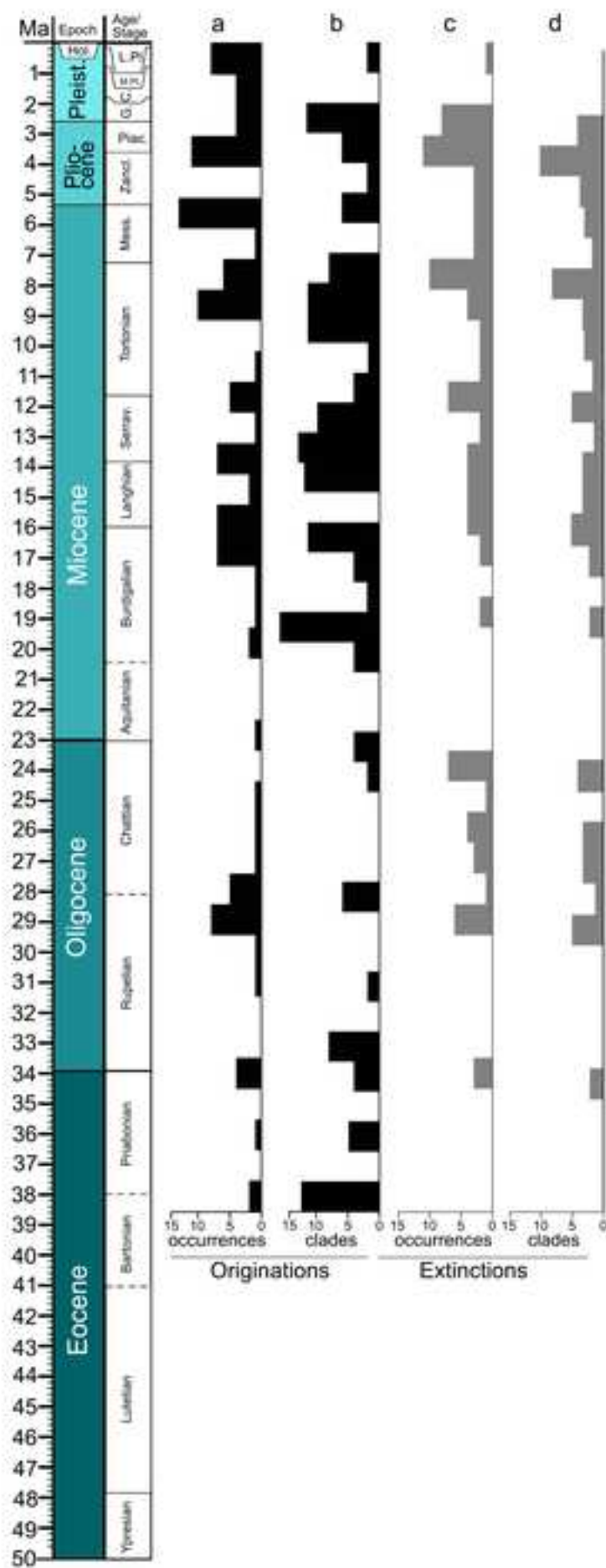




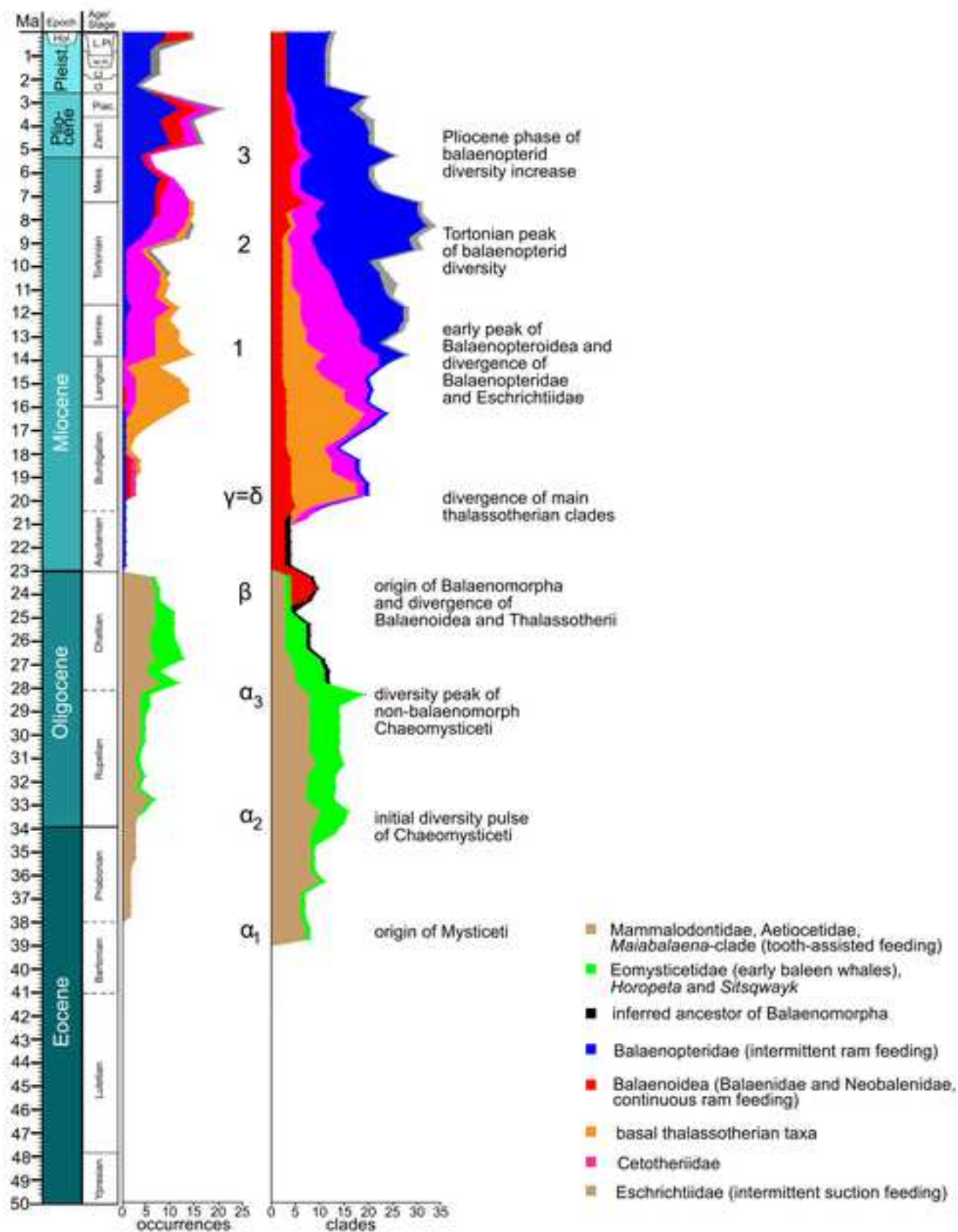


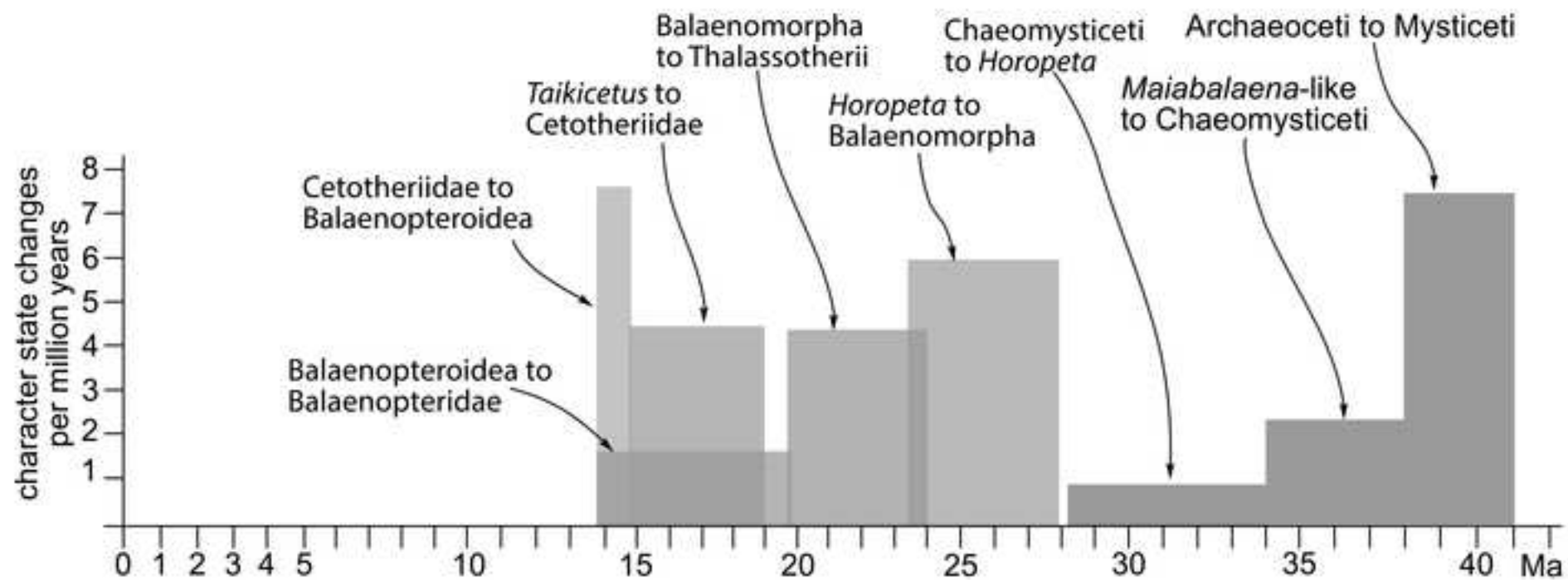


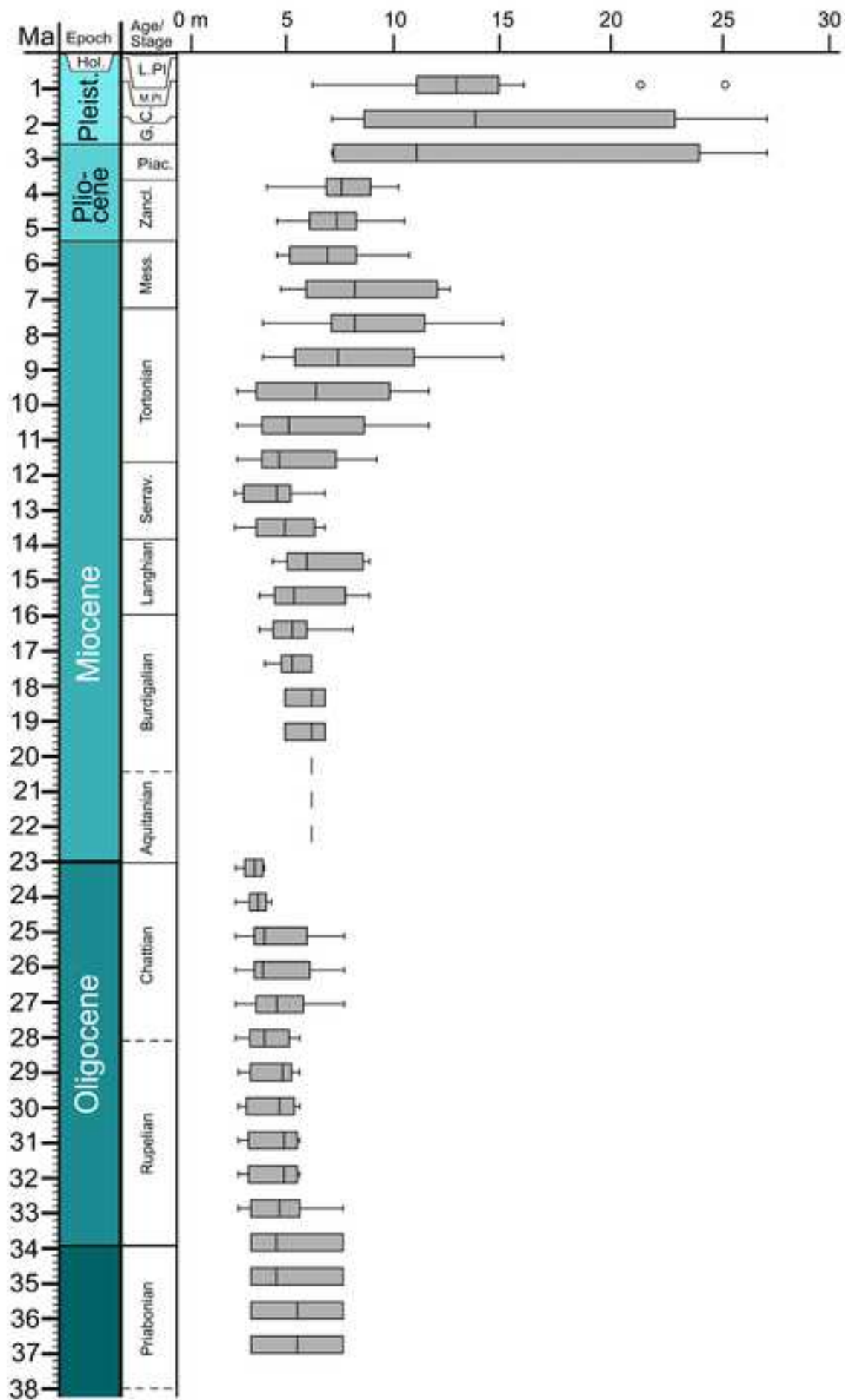












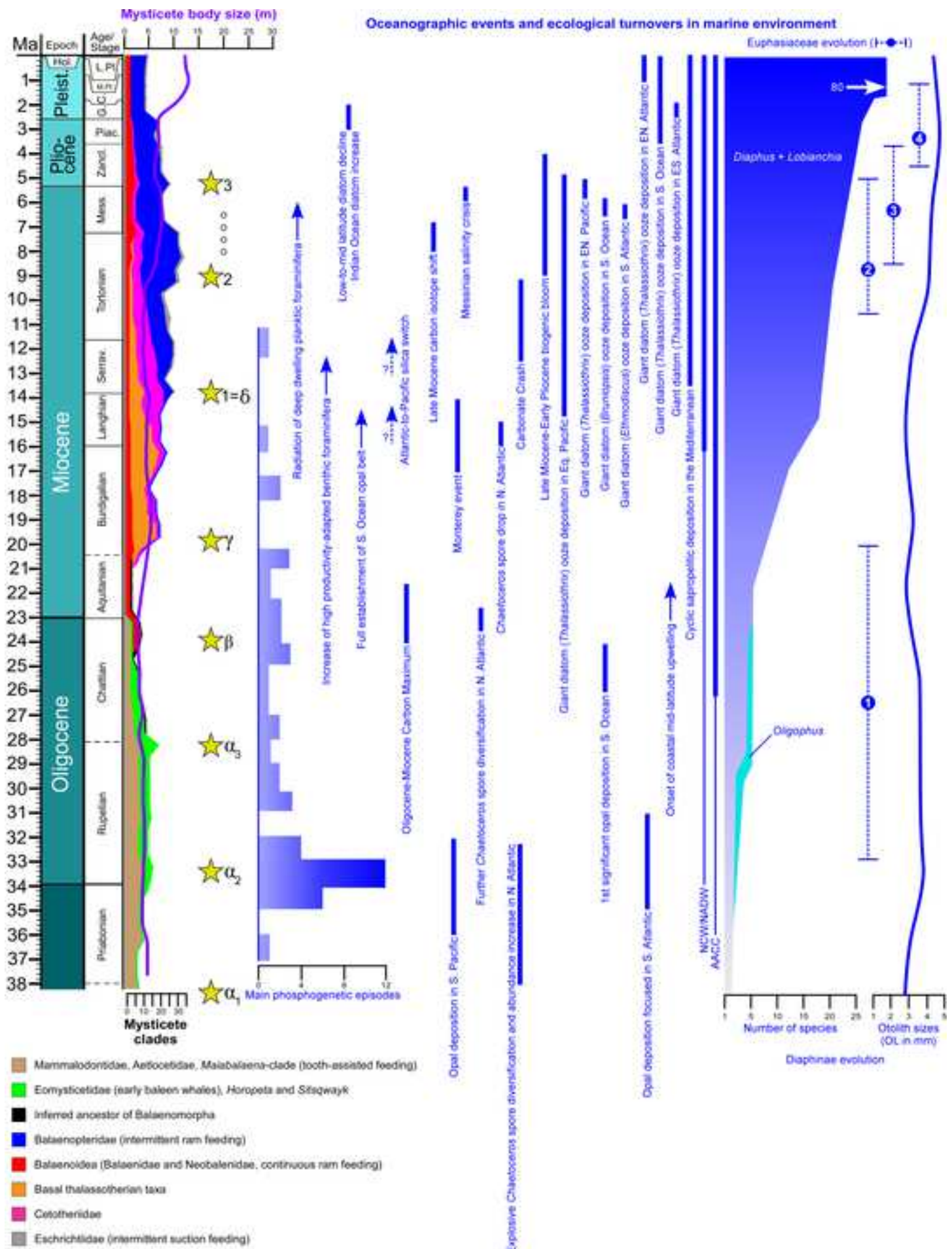












**Declaration of interests**

The authors declare that they have no known competing financial interests or personal relationships that could have appeared to influence the work reported in this paper.

The authors declare the following financial interests/personal relationships which may be considered as potential competing interests:





16 **Abstract**

1  
2  
3  
4  
5  
6  
7  
8  
9  
10  
11  
12  
13  
14  
15  
16  
17  
18  
19  
20  
21  
22  
23  
24  
25  
26  
27  
28  
29  
30  
31  
32  
33  
34  
35  
36  
37  
38  
39  
40  
41  
42  
43  
44  
45  
46  
47  
48  
49  
50  
51  
52  
53  
54  
55  
56  
57  
58  
59  
60  
61  
62  
63  
64  
65

A comprehensive revision of the localities of discovery of fossil mysticetes is presented together with a highly inclusive phylogenetic analysis in order to provide the basis for a chronology of the main mysticete diversification events. The results suggest that the origin of Mysticeti (that include earlier toothed taxa together with today baleen-bearing cetaceans) occurred *c.* 38 Ma; the origin of Chaeomysticeti (that include only baleen-bearing cetaceans) occurred *c.* 28 Ma; the origin of Balaenomorpha (crown mysticetes) occurred *c.* 23.3 Ma. Additional chronological inferences are provided. Within this chronological framework, we analyzed diversity trends, origination and extinction patterns and body size evolution, and looked for eventual causal relationships between evolutionary processes, marine and terrestrial ecological turnovers and geodynamic events. We found five main diversification events corresponding to peaks in originations and, in a few cases, with the origin of different feeding strategies adopted by the different mysticete families. We found that different mechanisms are correlated to specific diversification events and these include changes in temperature and ocean circulation patterns, nutrient availability in the water column and diatom abundance and diversity. Resuming, no single mechanism explains all the diversification events occurred during mysticete evolution; rather, we found that each diversification event was correlated to different combinations of biotic and abiotic factors, suggesting that this group experienced major adaptation process to the changing paleoenvironments in the last 38 Ma.

66 **Key words**

67  
68  
69  
70  
71  
72  
73  
74  
75  
76  
77  
78  
79  
80  
81  
82  
83  
84  
85  
86  
87  
88  
89  
90  
91  
92  
93  
94  
95  
96  
97  
98  
99  
100

Baleen whales, Body size, Chronology, Diversity, Extinction/origination rates, Global change, Phylogeny, Trophic web evolution



## 1. Introduction

Extant mysticete cetaceans (i.e., baleen-bearing whales) are represented by a handful of species in six genera (Bannister, 2009) but their role in oceanic ecology is of paramount importance. Several lines of evidence showed that mysticetes sequester enormous quantities of Carbon through their ability to perform mass predation on schooling shrimps and fish (Pershing and Stamietzkin, 2020); moreover, they fertilize the oceans by releasing iron and other nutrients contained in their feces so that mysticetes are able to indirectly control the abundance of their prey and the algal component of the oceanic trophic webs (Savoca et al., 2021).

The study of the fossil record revealed that the past mysticete diversity reached levels unrivalled in present time (Berta and Lanzetti, 2020; Bisconti et al., 2019; Marx and Uhen, 2010) suggesting that structural aspects of the oceanic ecosystems of the last million years should have been profoundly different from today. Genetic analyses revealed that the exceptionally high numbers of individuals were in existence slightly before the beginning of the industrial whaling (e.g., Roman and Palumbi, 2003; Rooney et al., 2001) in at least four species (*Balaena mysticetus*, *Balaenoptera acutorostrata*, *B. physalus* and *Megaptera novaeangliae*). This supports the view that we are living at a time of widespread ecological change due, at least partially, to a massive reduction in baleen whale abundance (e.g., Pershing et al., 2010). Understanding the past ecological settings when mysticetes were more abundant represents a good starting point to better understand both the evolutionary history of baleen whales and historical changes in ocean ecology.

Previous studies focused on past mysticete diversity and its relation to diatom abundance, temperature variability, major tectonic events, and nutrient availability in the oceans throughout the Cenozoic (e.g., Bisconti et al. 2021, 2019, 2010; Marx and Fordyce, 2015; Steeman et al., 2009; Marx and Uhen, 2010; Fordyce, 1980, 1977). The analyses led to hypotheses about the eventual existence of causal relationships between diversity and body size change in mysticetes and some paleoclimatic and paleoecological parameters, such as the temperature decline in the Pleistocene and the availability of nutrients supporting biogenic blooms in specific age intervals (Bisconti et al.,

68 2021; Slater et al., 2017; Marx and Uhen, 2010). Despite these efforts, several questions remain  
1  
2  
3 69 unanswered. It is still unclear the extent of the causal relationships between abiotic and biotic  
4  
5 70 factors in promoting or depressing the diversity of mysticetes in the past as it is not fully understood  
6  
7 71 the role that the fertilizing actions of the mysticete individuals can have had in the past oceanic  
8  
9 72 ecology. Following the theoretical framework of Berge et al. (2012) and the experimental works of  
10  
11  
12 73 Savoca et al. (2021), mysticetes should not be viewed only as passive actors in the oceanic  
13  
14 74 ecosystems but, rather, as active agents of ecosystem engineering able to shape the energy flow  
15  
16  
17 75 between the different parts of the trophic web.  
18  
19 76 To improve our understanding of the role of baleen whales within their ecosystems, a detailed  
20  
21  
22 77 analysis of their past diversity is necessary in the framework of a more accurate estimate of the  
23  
24 78 timings of their diversification. The latter is a key point because divergence dates of the main  
25  
26  
27 79 mysticete clades are crucial in the understanding of the rates of morphological evolution, rates of  
28  
29 80 body size change, and origination/extinction patterns (e.g., Katz, 2019; Alroy, 2014). In the last two  
30  
31  
32 81 decades, a number of works focused on the inference of divergence dates for major mysticete clades  
33  
34 82 and all were based on molecular or total evidence analyses (e.g., Árnason et al., 2018; Marx and  
35  
36 83 Fordyce, 2015; Geisler et al., 2011; Steeman et al., 2009; McGowen et al., 2009; Sasaki et al.,  
37  
38  
39 84 2005). In these studies, the fossil record was used for calibration of molecular clocks and the results  
40  
41 85 were highly variable. For example, based on molecular and total evidence analyses, the origin of  
42  
43  
44 86 crown mysticetes was inferred to range between 39 (late Eocene) and 29 (early Oligocene) Ma but  
45  
46 87 newly discovered fossils provided evidence that the earliest mysticetes were existent at least since  
47  
48  
49 88 33 Ma (Fordyce and Marx, 2018; Muizon et al., 2017) thus excluding a younger age for the origin  
50  
51 89 of crown Mysticeti. Again, this undermines the sensitivity of molecular clocks to updated  
52  
53  
54 90 knowledge of the fossil record.  
55  
56 91 To overcome the problems related to the molecular clocks, we investigated the possibility to infer  
57  
58 92 divergence dates for main mysticete clades by using a statistical method described by Gingerich and  
59  
60  
61 93 Uhen (1998) and subsequently used by Bajpai and Gingerich (1998) and O’Leary and Uhen (1999)

94 to infer the divergence date of Cetacea from their terrestrial ancestors. The method uses occurrence  
1  
2 data (number of localities) to make statements about presence/absence of a given taxon in a given  
3  
4  
5 stratigraphic range within an interval of statistical significance. We outline this method in the  
6  
7 Material and methods section and direct the reader to O’Leary and Uhen (1999) for a detailed  
8  
9 explanation. As detailed occurrence and locality data are available from the Paleobiology Database,  
10  
11 we used this method in order to infer the divergence dates of the main mysticete clades including  
12  
13  
14 Mysticeti, Chaemysticeti (baleen-bearing whales), Balaenomorpha (crown Mysticeti), Balaenoidea  
15  
16 (right and pygmy right whales), and Balaenopteroidea (rorquals, humpbacks and grey whales). We  
17  
18 then used the new divergence dates to assess several parameters emerging from the mysticete fossil  
19  
20 record: (a) origination/extinction patterns, (b) diversity patterns, (c) rates of morphological change,  
21  
22 and (d) rates of body size change. In the end, we compared our results with data from diatom  
23  
24 abundance and diversity, temperature variability, tectonic events, and nutrient availability in order  
25  
26 to obtain an integrated view of the possible drivers that concurred to mysticete diversity and  
27  
28 evolution throughout most of the Cenozoic.  
29  
30  
31  
32

33 The advantage of using this method is that it provides ranges of divergence dates that are fully  
34  
35 independent from models of molecular evolution and thus it does not suffer from well-known  
36  
37 shortcomings of the molecular clocks (see, e.g., Bromham, 2019; Katz, 2019). The disadvantage  
38  
39 consists in that the confidence interval of first and last occurrence data for the taxa may be low  
40  
41 because it depends on uncertainties about the beginning and duration of worldwide sedimentary  
42  
43 processes (Alroy, 2014). To overcome this problem, a detailed review of the mysticete-bearing  
44  
45 localities was performed allowing the compilation of the most accurate dataset.  
46  
47  
48  
49

50 A new and comprehensive phylogenetic analysis of mysticetes was necessary to enable us to  
51  
52 contextualize our chronological results within a phylogenetic framework, including as many taxa as  
53  
54 possible from as many worldwide localities as possible. Within such a comprehensive phylogenetic  
55  
56 framework, we aim at (1) describing the main evolutionary events (morphological change,  
57  
58 extinction/origination patterns, body size change) occurred during mysticete evolution, and (2)  
59  
60  
61  
62

120 investigating into the possible causal relationships between these events and other biotic and abiotic  
1  
121 factors to better understand the evolution of the oceanic ecological webs in the last 40 million years.

122

## 123 **2. Materials and methods**

124

### 125 *2.1. Structure of the dataset*

126 The data used in the present paper are available as supplementary online materials. We provided  
127 two files (Supplementary File 1 and 2) including what follows. In the Supplementary File 1, we  
128 provide data on specimens (repositories, accession numbers, stratigraphic ages, geographic ranges,  
129 body size, discussion on localities, body size inference of *Llanocetus denticrenatus*, and relevant  
130 literature), the character states and matrix used in the phylogenetic analysis. Moreover, in  
131 Supplementary File 1, links to the research results of the Paleobiology Database are provided in  
132 order to show the outputs of our searches in formats generated by the Paleobiology Database itself.  
133 In the Supplementary File 2, we provide the dataset compiled for the analysis of body size change  
134 in each mysticete family-rank taxon; the dataset is provided in a format readable by PAST  
135 (Hammer et al., 2001) and must be opened from within the PAST environment. The same data are  
136 also reported in Word in the Supplementary File 1 and can be read outside the PAST environment.

### 138 *2.2. Phylogenetic analysis*

139 We realized a new phylogenetic analysis of Mysticeti including 367 morphological characters  
140 scored for 98 Operational Taxonomic Units (hereinafter: OTU). The characters were mainly  
141 osteological and the character list is provided in Table S1 (Supplementary File 1). Currently, this is  
142 the most inclusive phylogenetic analysis of Mysticeti ever attempted up to now. The character x  
143 taxon matrix is presented in Table S2 (Supplementary File 1). The dataset was assembled based on  
144 the specimens listed in Table S3 and on the literature provided therein (see also Table S4 for  
145 institutional abbreviations used throughout the paper; Supplementary File 1). We used TNT

146 (Goloboff and Catalano, 2016) for phylogenetic inference. We used commands to hold 5000  
1  
147 cladograms in memory and then we performed 2000 random addition sequences of tree bisection  
2  
3  
4  
148 reconnection algorithm (hereinafter: TBR) as implemented in TNT with 10 trees saved per  
5  
6  
149 replication. We assessed the morphological support at nodes by bootstrap (1000 replicates) and  
7  
8  
150 symmetric resampling (absolute frequencies; 33 change probability; 1000 replicates). A strict  
9  
10  
151 consensus (Nelsen) tree was calculated by TNT based on the most parsimonious cladograms found  
11  
12  
13  
14  
152 by the analysis. Both Consistency (CI) and Retention (RI) indices were calculated by TNT; the  
15  
16  
153 Homoplasy Index ( $HI = 1 - CI$ ) was calculated by hand. To visually assess the number of  
17  
18  
19  
154 supporting synapomorphies at nodes, we computed a phylogram using MESQUITE 3.61 (Maddison  
20  
21  
22  
155 and Maddison, 2019).  
23  
24  
156 Finally, to assess the agreement between the branching pattern of the phylogenetic result and the  
25  
26  
157 stratigraphic ages of the OTUs, we calculated the Stratigraphic Consistency Index (SCI) that is  
27  
28  
158 defined as (number of stratigraphically-consistent nodes)/(expected total number of nodes)  
29  
30  
31  
159 (Huelsenbeck, 1997; see also Bisconti, 2007 for a discussion of pros and cons of using this index in  
32  
33  
160 mysticete phylogenetics).  
34  
35

### 36 37 38 39 40 41 42 43 44 45 46 47 48 49 50 51 52 53 54 55 56 57 58 59 60 61 62 63 64 65

2.3. *Assessment of clade ages*

163 Stratigraphic distributions of the mysticete taxa are provided in Table S3 (Supplementary File 1);  
164 the ranges in the table are used to realize Fig. 1 that will help to visualize the temporal abundance of  
165 mysticete species. It must be remarked that most of the past diversity of mysticetes is represented  
166 by species known only by one specimen (the holotype). In these cases, the stratigraphic distribution  
167 corresponds to the error of the estimation of the geological age of such a specimen. In those cases in  
168 which more specimens are known for the species, the stratigraphic distributions correspond to First  
169 Appearance Data (FAD) and Last Appearance Data (LAD) in the classical meanings of these terms.  
170 Various methods have been developed to statistically assess the minimum and maximum  
171 stratigraphic age of a clade based on its fossil record (reviewed by Wang and Marshall, 2016;

172 Rivadeneira et al., 2009). Statistical analyses rely on models describing the expected distribution of  
 1  
 173 the fossil record and the diversification trends of the taxa under investigation (Wang and Marshall,  
 2  
 174 2016 and literature therein). Gingerich and Uhen (1998) discussed the models that could be applied  
 3  
 4  
 5  
 6  
 175 to a statistical analysis of the time of origin of the Cetacea in great detail and observed that some of  
 7  
 8  
 9  
 176 the models necessary for the application of a number of statistical equations have to be relaxed in  
 10  
 11  
 12  
 177 order to get a thorough analysis of the cetacean fossil record. In particular, they discussed the  
 13  
 14  
 178 applicability of the equation of Strauss and Sadler (1989) to determine the timing of the origin of  
 15  
 16  
 179 Cetacea based on the stratigraphic assessment of the fossil record of the Archaeoceti,  
 18  
 19  
 180 Mesonychidae and Hapalodectidae. The equation is based on an assessment of the Observed  
 20  
 21  
 181 Temporal Density (OTD, that is the temporal range of a given taxon as documented by its fossil  
 22  
 23  
 182 record and quantified by the time of its first and last appearances in the stratigraphic record), the  
 24  
 25  
 183 Expected Temporal Density (ETD, that is the temporal range in which we expect to find fossils of a  
 26  
 27  
 28  
 284 given taxon), the number of localities independently sampled in which fossils of the investigated  
 29  
 30  
 31  
 185 group are found ( $n$ ) and a probability level ( $\lambda$ ) that can be set at 0.05 in order to have a statistically  
 32  
 33  
 34  
 186 significant estimation of the time of origin. Equation (1) represents the Strauss and Sadler (1989)  
 35  
 36  
 187 equation:

$$(1) \quad \lambda = \left(\frac{OTD}{ETD}\right)^{n-1}$$

189 By resolving Equation (1), the ETD of a group can be inferred as follows:

$$(2) \quad ETD = \frac{OTD}{n-1\sqrt{\lambda}}$$

191 where OTD is the observed temporal range obtained by the fossil record,  $n$  is the number of the  
 192 localities where the fossils were independently sampled and  $\lambda$  is the level of statistical significance  
 193 ( $\lambda = 0.05$ ). Equation (2), thus, provides an estimation of the timing of origin of a taxon based on its  
 194 observed temporal range as drawn from the stratigraphic ages of its fossil record in the sampled  
 195 localities. Following the mathematical implementation of this formula by Gingerich and Uhen



196 (1998), the assumption of a uniform distribution of the fossils throughout the ETD can be ignored  
1  
197 as we are interested in determining the timing of origin of a group and not its whole time span.  
2  
3  
4  
198 Here, our purposes are to determine the time of origin of Chaeomysticeti, Balaenomorpha,  
5  
6  
199 Thalassotherii, basal thalassotherians, Cetotheriidae, Balaenoidea, Balaenidae, Neobalaenidae,  
7  
8  
200 Balaenopteroidea, Eschrichtiidae and Balaenopteridae (Table S5). We downloaded the stratigraphic  
9  
10  
11  
1201 data from the Paleobiology Database by searching for these groups (see paragraph 2.1. *Structure of*  
12  
13  
14  
202 *the dataset*). The time of first occurrence and the time of last occurrence (respectively: FAD and  
15  
16  
1203 LAD for species known based on more than one specimen, and lower and higher limits of the error  
17  
18  
19  
204 of estimations of the geological ages of species represented by the holotype only) of the taxa were  
20  
21  
205 computed (Table S3) and then the equation (2) was resolved in order to provide an estimation of the  
22  
23  
206 time of origin of each of the investigated clades. The ages of all the taxa used in the phylogenetic  
24  
25  
207 analysis are provided in Table S3.  
26  
27  
28

#### 209 2.4. *Rates of morphological evolution*

210 We used MESQUITE 3.61 to find the morphological transformations at nodes. We counted the  
211 maximum number of transformations for each node and then divided this number by the estimated  
212 duration of the ramus connecting the clade under investigation and the ancestor shared with its  
213 closest sister group in order to get an estimation of the mean number of morphological  
214 transformations per million years. Our phylogenetic analysis used an ACCTRAN optimization  
215 algorithm; following Brusatte et al. (2011), both ACCTRAN and DELTRAN algorithms provide  
216 similar morphospaces, therefore, the choice of one or the other is not strictly relevant to our goals.  
217 We then realized a histogram showing the cumulative number of morphological transformations  
218 detected in all the investigated lineages in order to find time intervals of accelerated or reduced  
219 morphological evolution.  
220

220 We did not include autapomorphies in our dataset. We are aware that the autapomorphies play an  
221 important role in determining rates of morphological evolution but our work focuses on the origin

222 and evolution of main mysticete clades and not on single species, therefore the role of  
1  
223 autapomorphies would not provide crucial detail in our analysis, justifying our decision to exclude  
3  
4  
224 them. To corroborate this point, we follow the results of Smith et al. (2021) who, in their analysis of  
6  
225 disparity patterns, found that the internal branches of a cladogram characterize synapomorphic  
8  
9  
226 character evolution and predict the dispersal of taxa within the morphospace. On the contrary,  
10  
11  
1227 terminal branches express the evolution of autapomorphies, predict the margin of the morphospace  
13  
14  
228 in which terminal taxa will diverge and increase the length of the terminal branches (Smith et al.,  
15  
16  
1229 2021; Matzke and Irmis, 2016). We are interested in the origin of main mysticete clades and,  
18  
19  
230 therefore, the distribution of synapomorphic characters across internal nodes is our focus. As  
20  
21  
231 autapomorphies play no role in this kind of research, we did not include autapomorphies in our  
23  
24  
232 dataset.

25  
26  
233 To better visualize the distribution of synapomorphies at the internal nodes of the cladogram, we  
27  
28  
234 realized a phylogram by using MESQUITE 3.61. In the phylogram, the length of each ramus is  
30  
31  
235 proportional to the number of the inferred morphological transformations.

### 32 33 34 35 36 37 2.5. Rates of body size change

38  
39  
40  
41  
42  
43  
44  
45  
46  
47  
48  
49  
50  
51  
52  
53  
54  
55  
56  
57  
58  
59  
60  
61  
62  
63  
64  
65

Bisconti et al. (2021) analyzed the evolution of body size in right and bowhead whales (*Balaenidae*) and provided a rationale to define different size classes for mysticete whales. Their rationale represents a synthesis of morphometric and physiological works resulting from different research strategies (e.g., Goldbogen et al., 2019; Marx et al., 2019; Slater et al., 2017; Fordyce and Marx, 2018). We adopted the following definitions provided by Bisconti et al. (2021): small-sized species, body length < 8 m; medium sized species, body length between 9 and 13 m; large-sized species, body length between 14 and 20 m; and gigantic species, body length > 20 m. Bisconti et al. (2021) justified the restriction of the term ‘gigantic’ to only species with total body length (hereinafter, TL) > 20 m based on the observations of Goldbogen et al. (2019) that only three of the extant species (i.e., *Balaenoptera musculus*, *Balaenoptera physalus* and *Megaptera novaeangliae*) may attain

248 more than 20 m in TL thanks to peculiar abilities to engulf enormous quantities of high-energy  
1  
249 prey. These three species are among the largest animals that ever lived in our planet (Slater et al.,  
3  
4  
250 2017; Pyenson and Sponberg, 2011).  
6  
251 Our assessment of TL in extinct mysticetes is largely based on the results published by Bisconti et  
8  
9  
252 al. (2021) and Slater et al. (2017) for the Balaenoidea and the other non-balaenoid mysticetes,  
10  
11  
253 respectively. Taxa that were not assessed in these works but that are included in the present study  
13  
14  
254 are non-balaenoid ones and their TL is assessed herein by applying the formula provided by Slater  
15  
16  
255 et al. (2017) for stem-balaenopterids. The TL of the taxa included in the present work are provided  
18  
19  
256 in Table S6 (Supplementary File 1).  
20  
21  
257 To quantitatively assess the rate of TL change across the mysticete phylogeny, we reconstructed the  
23  
24  
258 TL at ancestral nodes by maximum parsimony inference as implemented in MESQUITE 3.61.  
25  
26  
259 Changes occurred in TL in the different mysticete families were represented by box plots vs time.  
27  
28  
260 Our study of body size evolution in mysticetes is not based on an *a priori* assumption of linear  
30  
31  
261 variation through time. The distribution of TL values through time is the only datum on which we  
32  
33  
262 make observations and analyses.

## 263 264 2.6. Diversity change throughout mysticete evolution

40  
41  
265 The diversity (in terms of species number) of mysticete clades was graphically assessed by plotting  
42  
43  
266 the number of species present in time bins of 0.5 Ma based on the fossil record and on cladistic  
44  
45  
267 results. We analyzed the mysticete species known in the fossil record from data downloaded from  
47  
48  
268 the Paleobiology Database and available from Supplementary File 2. Assessments of extinction and  
49  
50  
269 origination rates were performed by plotting the number of earliest and latest occurrence of taxa  
52  
53  
270 (based on LAD and FAD of species represented by more than one specimen, and on lower and  
54  
55  
271 upper limits of the error of the estimation of the geological ages of species represented by the  
57  
58  
272 holotype only) vs time in time bins of 1 Ma. Finally, the diversity of different families was plotted  
59  
60  
273 vs time to realize a sort of illustration of ‘evolutionary faunas’ in the sense of Sepkoski et al. (1981;

274 see also Droser 2003) to help visualizing possible competitive relationships between families. As  
1  
275 usual, in the case in which the diversity of a single family declines at the same time when that of  
3  
276 another family increases, then a process of competition-driven extinction is observed. We plotted  
4  
6  
277 both the actual fossils depicting the diversity of known families and clades based on our  
8  
278 phylogenetic results vs time.  
10

11  
1279

## 14 280 *2.6. Relationships to Cenozoic global changes*

16  
1281 Patterns of body size and morphological evolution were compared with published geochemical,  
18  
19 282 paleontological and sedimentological proxies of paleoclimatic and paleoceanographic changes  
20  
21 283 occurred throughout the Cenozoic, with the aim of highlight possible relationships. Particular  
22  
23 284 attention has been given to planktic diatoms (Bacillariophyceae), i.e. silica-shelled unicellular  
24  
25 285 primary producers at the base of the marine trophic chain on which mysticetes rely (e.g., Kooistra et  
26  
27 286 al., 2007), and to the abiotic and biotic factors that controlled their abundance from the Eocene  
28  
29 287 onward.  
30  
31  
32

33  
3488

## 36 389 **3. Results**

37  
38  
3990

### 41 491 *3.1. Revisions of localities*

42  
43 492 We checked more than 1400 localities for fossil mysticetes that are reported in the Paleobiology  
44  
45 493 Database. The localities are provided in the dataset published online in the Supplementary File 3.  
46  
47 494 We dismissed some localities following specific discussions as reported in the notes to the Table S5  
48  
49  
50  
51 495 (Supplementary File 1).  
52

53 496

### 55 497 *3.2 Phylogenetic analysis*

56  
57  
58 498 The results of the phylogenetic analysis are shown in Fig. 2 where the strict consensus of 26 most  
59  
60 499 parsimonious cladograms is presented. The most parsimonious solution is 1991 steps in tree length;  
61

300 it has a Consistency Index (CI) of 0.247, a Retention Index (RI) of 0.736 and an Homoplasy Index  
1  
301 (HI) of 0.753.  
3  
4  
302 The present analysis recovers Mysticeti as a monophyletic group. Earliest diverging mysticetes are  
6  
303 the Mammalodontidae, followed by *Fucaia* and *Aetiocetus* representing the most plesiomorphic,  
8  
304 toothed mysticetes known up to now. A clade formed by *Llanocetus*, *Maiabalaena*, *Toipahautea*,  
10  
11  
305 *Mystacodon* and *Coronodon* is detected here for the first time and is referred herein to as  
13  
14  
306 *Maiabalaena*-like group. This clade is the sister group of *Tohoraata raekoao* that is, in turn, the  
15  
16  
307 sister group of the Chaeomysticeti (including all the baleen-bearing mysticetes). The  
18  
19  
308 Eomysticetidae are the basal-most chaeomysticetes and represents the family-rank group that is  
20  
21  
309 closer to Balaenomorpha (including all the extant mysticete families). Interposed between  
22  
23  
310 Eomysticetidae and Balaenomorpha are two Oligocene taxa, *i.e.*, *Sitsqwayk cornishorum* and  
25  
26  
311 *Horopeta umarere*. *Sitsqwayk* is the sister group of the Balaenomorpha.  
27  
28  
312 Balaenomorpha is split into two large monophyletic groups: Balaenoidea (including Balaenidae and  
30  
31  
313 Neobalaenidae) and Thalassotherii (including basal thalassotherian taxa, Cetotheriidae and  
32  
33  
314 Balaenopteroidea). The basal thalassotherian taxa are recognized as monophyletic herein and form a  
35  
36  
315 family-rank clade that still has to receive a formal denomination. Several subgroups of basal  
37  
38  
316 thalassotherians are detected and could represent distinct subfamilies but we abstain from providing  
40  
41  
317 new names as additional comparative information is necessary to further test the long debated  
42  
43  
318 monophyly of this group. *Taikicetus* is the sister group of Cetotheriidae + Balaenopteroidea  
44  
45  
319 (including Eschrichtiidae and Balaenopteridae). Eschrichtiidae is a monophyletic group excluded  
47  
48  
320 from being part of Balaenopteridae.  
49  
50  
321 Bootstrap support values and symmetric resampling values (shown in Fig. 2) show support for most  
52  
53  
322 of the main mysticete clades described above. In particular, strong support is found for the  
54  
55  
323 monophyly of the Mysticeti, Balaenomorpha, Balaenoidea, Eomysticetidae, Balaenidae and  
57  
58  
324 Neobalaenidae. In the present analysis, the other family-rank clades received less than 50% from  
59  
60  
325 both bootstrap and symmetric resampling. Low bootstrap supporting values may depend on several  
62  
63  
64  
65

326 factors. In particular, bootstrap values are inversely proportional to (1) number of characters of the  
1  
327 dataset, (2) number of autapomorphies, (3) number of non-informative character states for a given  
3  
4  
328 node, and (4) increased taxon sample. In our dataset, both the taxonomic and morphological  
6  
329 samples are quite high thus leading to reduced bootstrap supporting values. A certain degree of  
8  
330 homoplasy, as testified by CI, RI and HI, together with question marks in the matrix certainly  
10  
11  
1331 contributed to lower the bootstrap supporting values.  
13  
14  
332 Additional >50% supporting values are found for the monophyly of *Atlantictetus*, *Echrichtius* +  
15  
16  
1333 *Eschrichtioides*, '*Balaenoptera*' *cortesii* var. *portisi*, *Protororqualus* and *Incakujira*. Other  
18  
19  
1334 relationships are too poorly supported by bootstrap and symmetric resampling and the  
20  
21  
2335 corresponding values are not shown in Fig. 2.  
23  
24  
2336 A schematic representation of the relationships of the family-rank clades is shown in Fig. 3. Most of  
25  
26  
2337 the mysticete taxa known from the extant and the fossil record are included in a minimum of eight  
27  
28  
2338 family-rank clades, some of which still need to be denominated. A few species still fall outside the  
30  
31  
2339 family-rank clades including *Fucaia*, *Tohoraata*, *Horopeta*, *Sitsqwayk* and *Taikicetus*. These taxa  
32  
33  
2340 cannot be assigned to new families as additional morphological information is necessary to better  
35  
36  
2341 characterize most of them.  
37  
38  
2342  
40  
41  
42  
43  
44  
45  
46  
47  
48  
49  
50  
51  
52  
53  
54  
55  
56  
57  
58  
59  
60  
61  
62  
63  
64  
65

### 3.3. Chronology of main mysticete clades

We used the OTR values in Tables S3 and S5 to resolve Equation (2) for mysticete clades. The results are shown in Table 1 where OTR, ETR and observed and estimated clade stratigraphic ranges (respectively, OCSR and ECSR) are presented. The origin of Mysticeti is traced back to 38 Ma in the late Eocene; the time of origin of Chaeomysticeti is estimated being c. 34 Ma (latest Eocene-to-earliest Oligocene) suggesting that the origin of filter feeding occurred very quickly after the origin of the mysticete body plan. The origin of Balaenomorpha is estimated c. 23.3 Ma at the beginning of the Miocene when all the main crown mysticete clades (i.e., Balaenopteroidea, Balaenoidea and Thalassotherii) occur in the fossil record.



352 We estimated also the time of origin and stratigraphic durations of family-rank taxa including  
1  
353 Eomysticetidae (ECSR: 29.2-20.4 Ma), Thalassotherii (ECSR: 23.11-0 Ma), Cetotheriidae (19.8-0.8  
3  
4  
354 Ma), basal thalassotherian taxa (ECSR: 24-7.1 Ma), Balaenopteroidea (ECSR: 20-0 Ma) and  
6  
355 Balaenopteridae. The ECSR of these clades allowed to infer clade durations (Table 1) that were  
8  
356 used for the calculus of rates of morphological and size change.

357 We plotted the simplified version of the mysticete phylogeny of Fig. 3, including only family-rank  
13  
358 taxa, against a time scale and presented the result in Fig. 4. Four main diversification events are  
15  
359 detected from our chronological reconstructions. We named these events with Greek letters and  
18  
360 numbers following the scheme proposed by Bisconti et al. (2019). Our results suggest that the first  
20  
361 event of Bisconti et al. (2019) is to be splitted into two different events. In fact, while in Bisconti et  
23  
362 al. (2019) resolution was too low to unravel the structure of the first event ( $\alpha$  event of Bisconti et al.  
25  
363 2019), here we performed a more detailed analysis that allowed us to dissect this event and find that  
28  
364 it is actually formed by two distinct sub-events. We decided to maintain the names of the main  
30  
365 events as provided by Bisconti et al. (2019) and designed two sub-events deriving from the splitting  
32  
366 of the  $\alpha$  event ( $\alpha_1$  and  $\alpha_2$ ). The first,  $\alpha_1$  represents the origin of Mysticeti; the second,  $\alpha_2$ , represents  
35  
367 the origin of the Chaemysticeti.

368 This reconstruction implies that the process of assembly of the chaemysticete characters occurred  
40  
369 in *c.* 10 million years and that additional stem-Chaemysticeti are expected to occur in the time  
42  
370 interval between 34 (inferred origin of Chaemysticeti) and 28 (origin of chaemysticete whales  
45  
371 such as Eomysticetidae) Ma.

372 The  $\beta$  event in the late Chattian (late Oligocene) represents the origin of Balaenomorpha or crown  
50  
373 mysticetes. It marks the divergence between the Balaenoidea and the Thalassotherii, and represents  
52  
374 a major event in that two different filter feeding groups, characterized by profoundly different  
55  
375 feeding styles, diverged from a common ancestor: the continuous ram feeders (Balaenoidea) and the  
57  
376 intermittent ram feeders (including extant Balaenopteridae and, possibly, both basal Thalassotherian  
59  
377 taxa and Cetotheriidae). By implication, it is expected that the stem-Thalassotherii were in existence

378 from the inferred divergence time corresponding to the  $\beta$  event even in the absence of fossil  
1  
379 evidence, as the earliest fossil thalassotherians date back to the Burdigalian, early Miocene (*c.* 20  
3  
380 Ma), about 4 million years after the inferred divergence time from the common ancestor shared with  
6  
381 Balaenoidea.

382 The  $\gamma$  event corresponds to the splitting of Thalassotherii into three different clades: basal  
10  
383 thalassotherian taxa, Cetotheriidae and Balaenopteroidea. It occurred approximately at the  
13  
384 Aquitanian/Burdigalian boundary around 20 Ma. The Cetotheriidae originated from its sister group  
15  
385 during the  $\gamma$  event. *Prototorqualus dyticus* (Cabrera, 1926) from the early Miocene of Argentina  
18  
386 marks the early origin of Balaenopteroidea (according to Bisconti and Bosselaers, 2021) in the  $\gamma$   
20  
387 event.

23  
388 Bisconti et al. (2019) designated the  $\delta$  event occurred at the transition between Langhian and  
25  
389 Serravallian in the middle Miocene (*c.* 14 Ma) as marking the origin of Balaenopteroidea and the  
27  
390 divergence of Eschrichtiidae and Balaenopteridae. Our analysis supports the view that the origin of  
30  
391 Balaenopteroidea is part of the  $\gamma$  event and for this reason we labeled the  $\gamma = \delta$  event in Fig. 4.  
32

33  
392 Therefore, the  $\delta$  event of Bisconti et al. (2019) is abandoned here.  
35

### 393 394 3.4. Patterns of extinctions and originations

40  
395 In Fig. 5, we show the diversity of mysticetes based on fossil occurrences (Fig. 5A) and inferred  
42  
396 clade presence (Fig. 5B). Both graphs show approximately the same pattern that can be summarized  
45  
397 as follows: (i) an early phase of diversity expansion that started in the Priabonian and ended at the  
47  
398 end of the Chattian; (ii) a phase of reduced diversity in the stratigraphic interval in the Aquitanian;  
49  
399 (iii) a new phase of diversity increase from the Burdigalian to the end of the Pliocene punctuated by  
52  
400 additional events of diversity loss and increase. In Fig. 5B, clade diversity abruptly increased *c.* 9  
54  
401 Ma and dropped again around 7 Ma. In both graphs the origin of the modern mysticete species is  
57  
402 part of a process of diversity increase.  
59

403 Increases and decreases of diversity are analyzed in light of origination and extinction patterns in  
1  
404 Fig. 6 on scale of 1 million years. In the earliest phases of mysticete existence, originations are  
3  
405 scattered along a time interval of *c.* 10 million years between the Priabonian and the Chattian when  
4  
5  
6  
406 scarce extinction events are recorded in both the fossil record and clade durations. Evident  
8  
9  
407 extinction pulses in this phase are observed between 29 and 23 Ma. This pattern may help to explain  
10  
11  
408 the diversity fall observed in the Aquitanian as shown in Fig. 5A,B. Interestingly, this pattern shows  
13  
14  
409 that when the earliest mysticete morphotypes went extinct, they were not replaced by new species in  
15  
16  
410 the same clades. Rather, the extinct species created vacant niches although it is unlikely that these  
18  
19  
411 niches were occupied by chaemysticetes as the feeding styles of the latter were very different from  
20  
21  
412 those of the earliest mysticetes. The key morphological synapomorphy of Chaemysticeti, in fact, is  
23  
24  
413 the presence of baleen (Bisconti and Carnevale, 2022) that allows the performance of filter feeding  
25  
26  
414 in contrast to the earliest mysticetes that used a combination of biting and suction to mainly prey  
27  
28  
415 upon fishes (Berta and Lanzetti, 2020). Possible overlap in feeding styles could have been present  
30  
31  
416 between the archaic, toothed-mysticetes and the chaemysticetes in the case in which the  
32  
33  
417 coexistence of teeth and baleen would be definitely accepted in Aetiocetidae (as proposed by  
35  
36  
418 Deméré et al., 2008 and reiterated by Ekdale and Deméré, 2021; and Gatesy et al., 2022). However,  
37  
38  
419 alternative hypotheses have been formulated, which must be further corroborated by convincing  
40  
41  
420 morphological evidence (e.g., Peredo et al., 2021, 2017; Hocking et al., 2017; Marx et al., 2016),  
42  
43  
421 excluding the possibility that teeth and baleen coexisted in the same species.  
45  
422 Starting from the Aquitanian/Burdigalian boundary, intense origination events are observed that  
47  
48  
423 occur at the same time as a number of extinction events. This is the common pattern observed in the  
49  
50  
424 stratigraphic interval between Burdigalian and today, and corresponds to one of the main diversity  
52  
53  
425 increases represented in Fig. 5A,B ( $\gamma$  event of Fig. 4). Higher rates of originations are observed  
54  
55  
426 between 15 and 12 Ma, 10 and 7 Ma, and between 4 and 2 Ma. Higher extinction rates are observed  
57  
58  
427 between 8 and 7 Ma, and 4 and 2 Ma. This origination/extinction pattern is also evident from Fig. 7,  
59  
60  
428 where the mysticete phylogeny presented in Fig. 2 is plotted against a time scale including data for  
61  
62  
63  
64  
65

429 originations and extinctions of each taxon based on Table S3 (Supplementary File 1). In this graph,  
1  
430 the extinctions of the earliest, toothed mysticetes group occurred in the middle-to-late Oligocene  
3  
431 and no branches overcome the Oligocene-Miocene boundary, as also observed in Fig. 5A,B. There  
6  
432 is an overlap of stratigraphic ranges of toothed-mysticetes and earliest chaeomysticetes during the  
8  
433 late Oligocene; the stratigraphic ranges of *Sitsqwayk* and *Horopeta* demonstrate that also the stem-  
10  
11  
434 Balaenomorpha were present in the late Oligocene. The origin of Balaenomorpha is thus to be  
13  
14  
435 searched in the mid-to-late Oligocene. Judging from Fig. 7, stem-Balaenomorpha are expected to  
15  
16  
436 originate in the latest Rupelian (early Oligocene). The complete assembly of the synapomorphies of  
18  
19  
437 Balaenomorpha required *c.* 6 Ma and took place between 34 and 28 Ma (Fig. 7).  
20  
21  
438 The Miocene was the period with maximum mysticete diversity. Both the graphs in Fig. 5A,B and 7  
23  
24  
439 show that Balaenomorpha was a successful clade and that most of the known species were existent  
25  
26  
440 in the stratigraphic interval between Burdigalian and Tortonian. While there may be some sampling  
27  
28  
441 bias due to inadequate fossil record in Aquitanian and Messinian stages, the number of localities in  
30  
31  
442 which fossil mysticetes have been found corresponds to several hundred in the Aquitanian-  
32  
33  
443 Messinian interval, suggesting that the available information may be regarded as a reliable  
35  
36  
444 biological evidence. In this respect, Marx et al. (2019; see also literature therein) observed that there  
37  
38  
445 are several worldwide formations in which Aquitanian strata crop out that are rich in odontocete  
40  
41  
446 fossil remains but that bear a few or no mysticete fossils at all. The abundance of Aquitanian  
42  
43  
447 odontocetes rules out taphonomic artifact or significant sampling bias about the abundance  
45  
46  
448 assessment of Aquitanian mysticetes from the known localities. Marx et al. (2019) suggested that  
47  
48  
449 Aquitanian mysticetes (mainly belonging to Chaeomysticeti) moved offshore rather than remaining  
49  
50  
450 inshore as the pre-existent toothed mysticetes, and this prevented abundant fossilization due to the  
52  
53  
451 sedimentary and biotic characteristics of the oceanic floor in which complete destruction of whale  
54  
55  
452 skeletons is largely documented (see Dominici et al., 2020 for an extensive review of this process  
57  
58  
453 and further literature). This hypothesis could explain why aquitanian mysticetes are rare. In any  
59  
60  
61  
62  
63  
64  
65

454 case, it is apparent that Aquitanian localities are less numerous than localities from better sampled  
1  
455 time intervals and, therefore, a source of bias may still be present.

456 Several species went extinct at the Piacenzian/Gelasian boundary (c. 2.6 Ma) representing the end  
2  
457 of whole lineages (e.g., stem-balaenopterids) that were highly represented in the late Miocene and  
3  
458 Pliocene. The origination pulse observed in the Pleistocene in Fig. 5A,B and Fig. 7 is due to the  
4  
459 origin of the modern mysticete fauna (begun in the latest Miocene), including the genera  
5  
460 *Balaenoptera* and *Megaptera*, *Eschrichtius* and the extant right and bowhead whales (*Eubalaena*  
6  
461 *glacialis*, *E. australis*, *E. japonica* and *Balaena mysticetus*).  
7  
8  
9  
10  
11  
12  
13  
14  
15  
16  
17  
18  
19  
20  
21  
22  
23

### 463 3.5. Evolutionary faunas

464 We investigated the taxonomic composition of the mysticete diversity through time to understand  
24  
465 the proportional contribution that each family-rank clade provided to the global diversity pattern.  
25  
466 Our result is shown in Fig. 8. Both fossils (Fig. 8A) and branching pattern (Fig. 8B) show diversity  
26  
467 peaks and valleys consistent with the events described above. In the curves of Fig. 8, different  
27  
468 colors quantitatively represent the numbers of species belonging to each family-rank clade and  
28  
469 show the relative proportion of each of these clades during time intervals of 0.5 million years.  
29  
470 The initial diversification event of the mysticetes begun about 38 Ma with the early evolution of  
30  
471 toothed mysticetes; toothless and baleen-bearing mysticetes originated quickly after the initial  
31  
472 divergence of Mysticeti and maintained a comparable diversity with that of toothed taxa up to c. 23  
32  
473 Ma. No evident pattern of competition is observed in this phase (38-23 Ma) as toothed and baleen-  
33  
474 bearing mysticetes underwent similar diversification paths. An important extinction event occurred  
34  
475 at the Oligocene/Miocene boundary, c. 23 Ma, which affected both toothed and baleen-bearing taxa;  
35  
476 such an event was already recognized by Marx et al. (2019) and was evident in the analysis of the  
36  
477 mysticete diversity of Bisconti et al. (2019).  
37  
38  
39  
40  
41  
42  
43  
44  
45  
46  
47  
48  
49  
50  
51  
52  
53  
54  
55  
56  
57

478 The clade-based analysis of diversity, shown in Fig. 8B, suggests that the earliest Balaenomorpha  
58  
479 originated toward the end of the Chattian ( $\beta$  event) even though the fossil record documents their  
59  
60  
61  
62  
63  
64  
65

480 presence only from the Aquitanian (see Fig. 8A in which the  $\beta$  event is not recorded), with their  
1  
481 radiation that took place during the process that led toothed-mysticetes to the extinction. It is still  
2  
3  
4  
482 unclear whether the origin of Balaenomorpha triggered a competitive mechanism able to drive  
5  
6  
483 earliest mysticetes to disappear or not. More evident competitive patterns are observed in  
7  
8  
9  
484 subsequent phases and will be discussed below.  
10  
11  
1485 The  $\gamma$  event is mainly due to the expansion of the diversity of basal thalassotherians in the  
12  
13  
14  
486 Burdigalian and Langhian; all the other balaenomorph families marginally contributed to the total  
15  
16  
1487 diversity in the stratigraphic interval between 20 and 16 Ma. Starting from *c.* 16 Ma, there is an  
17  
18  
19  
488 increase in the diversity of Cetotheriidae that parallels a contemporaneous fall of the diversity of the  
20  
21  
22  
489 basal thalassotherians. The relationship between the increase in cetotheriid diversity and decrease in  
23  
24  
25  
490 basal thalassotherian diversity is evident from both fossil-based and clade-based analyses (Fig.  
26  
27  
28  
491 8A,B). This observation suggests an overlap in ecological preferences by these two family-rank  
29  
30  
31  
492 clades.  
32  
33  
34  
493 The rise of the Cetotheriidae was concluded when an expansion of the balaenopteroid diversity  
35  
36  
37  
494 occurs beginning from *c.* 13 Ma. The quick increase of balaenopteroid diversity sharply parallels  
38  
39  
40  
495 the fall of cetotheriid diversity and the extinction of the basal thalassotherian taxa *c.* 8 Ma. Such an  
41  
42  
43  
496 extinction occurred during the event 2 of Bisconti et al. (2019) in which the maximum  
44  
45  
46  
497 balaenopterid diversity is attained. Competitive mechanisms are evident from these curves  
47  
48  
49  
498 suggesting overlap between the ecological preferences of Balaenopteridae, Cetotheriidae and basal  
50  
51  
52  
499 thalassotherian taxa. Balaenopterids maintained a dominant contribution to the taxonomic  
53  
54  
55  
500 composition of the mysticete diversity through the whole Neogene with another pulse in diversity  
56  
57  
58  
501 (event 3: Pliocene) up to today. Interestingly, the clade-based analysis shows that the balaenid  
59  
60  
61  
502 diversity remained nearly constant through the last 23 million years with moderate peaks in the late  
62  
63  
64  
503 Miocene and Pliocene.  
65  
66  
67  
504 Bisconti et al. (2019) distinguished three diversification events of Balaenopteridae (see also Fig. 8).  
68  
69  
70  
505 The first event (No. 1) corresponds to the early diversification phase of basal rorquals. The second  
71  
72  
73  
74  
75

506 event (No. 2) corresponds to a Tortonian peak in mysticete diversity that is mainly due to a massive  
1 expansion of balaenopterid diversity; this peak is recognized as one of the most important  
507 diversification events in the history of mysticetes (Berta and Lanzetti, 2020; Bisconti et al., 2019;  
3  
4  
508 Marx and Fordyce, 2015; Marx and Uhen, 2010). The third event (No. 3) corresponds to a Pliocene  
6  
509 peak in diversity attained by both Balaenopteridae and Balaenidae recognized also by Berta and  
8  
510 Lanzetti (2020) and Marx and Uhen (2010).  
11

12  
13  
14  
15

### 1513 *3.6. Rates of morphological evolution*

1514 All the character state changes were reconstructed by MESQUITE that allowed inference of  
20  
21  
22  
23  
24  
25  
26  
27  
28  
29  
30  
31  
32  
33  
34  
35  
36  
37  
38  
39  
40  
41  
42  
43  
44  
45  
46  
47  
48  
49  
50  
51  
52  
53  
54  
55  
56  
57  
58  
59  
60  
61  
62  
63  
64  
65

1515 character states at ancestral nodes. We counted all the unambiguous character state changes along  
1516 selected branches in the phylogeny of Fig. 3 representing family-rank taxa and species that cannot  
1517 be included within any of the known families based on the phylogeny of Fig. 3. The changes were  
1518 subdivided by the duration of the branch as reconstructed from Table 1 and Figs. 4 and 7. The  
1519 results are presented in Fig. 9. We observed three different patterns: (1) the origin of the Mysticeti  
1520 was marked by a high number of morphological changes in a relatively short period of time (we  
1521 detected 22 morphological changes in 3 million years: 7.33 changes per million years); (2) the  
1522 transition from earliest, toothed mysticetes and chaeomysticetes was slow and gradual (6  
1523 morphological changes in 8.9 million years: 0.67 changes per million years); (3) the period between  
1524 28 and 14 million years was characterized by high rates of morphological changes. The latter  
1525 observation is consistent with the time constraints for the origin of Balaenomorpha (5.94 changes  
1526 per million years), Thalassotherii (4.31 changes per million years), Cetotheriidae (4.44 changes per  
1527 million years) and Balaenopteroidea (7.77 changes per million years).

1528 The rates described at point (3) occurred at the period in which the earliest-, toothed mysticetes and  
1529 Eomysticetidae decreased in diversity and eventually became extinct, and the origin of  
1530 Balaenomorpha and its subdivisions (Balaenoidea and Thalassotherii) occurred (Fig. 5). The high  
1531 number of extinction events occurring between 29 and 23 Ma and the high number of originations

532 occurring between 21 and 16 Ma (Fig. 6) suggest that an intense selective regime was acting on  
1  
533 mysticetes, during the time interval between 29 and 14 Ma, favoring the divergence of the main  
3  
4  
534 balaenoid and thalassotherian branches and the origins of the principal feeding styles of mysticetes.  
6

535

8

9

536

10

11

537

13

14

538

15

16

539

18

19

540

20

21

541

23

24

542

25

26

543

28

29

544

30

31

545

32

33

546

35

36

547

37

38

548

40

41

549

42

43

550

44

45

551

47

48

552

49

50

553

52

53

554

54

55

555

57

58

556

59

60

557

62

63

64

65

### 3.7. Body size evolution

We analyzed the distribution of body size in all the mysticete taxa investigated along their stratigraphic ranges. We recorded all the body sizes of the species in time intervals of one million years. The resulting box plot is shown in Fig. 10. Our analysis shows that mysticetes had small body sizes (TL included between *c.* 4 and *c.* 9 m) for most of their evolutionary history. In particular, toothed mysticetes were small-sized and never evolved medium-to-large size (this includes the holotype of *Llanocetus* whose TL does not exceed 9 m; we were unable to replicate the TL=12 m for the *Llanocetus* sp. specimen IAA Pv 731 based on the formulae used by Marx et al., 2019; our results range between 3.7 and 4.6 m for this specimen: see Supplementary Online Material Text S1). As shown in Fig. 10, a TL longer than 10 m is hardly observed in mysticetes before the early Tortonian (*c.* 10 Ma), which is still consistent with the observation of a more than 10 m long putative *Pelocetus* specimen still in the field in the Peruvian Pisco Formation, cursorily reported by Bianucci et al. (2019). Interestingly, rather than observing a clear trend toward longer TL values, our analysis shows a trend toward an expansion in body size range for mysticetes in the interval between Langhian and present. Pulses of increase in body size range are observed in the Langhian, Tortonian and Pliocene. The maximum increase in body size range is observed in the latest Pliocene and in the Pleistocene, with a neat drop in the last million year probably following the general trend toward diversity decrease observed in Fig. 8. In more recent times, the gigantic blue and fin whales (*Balaenoptera musculus* and *B. physalus*) represent outliers whose maximum TL values are not included within the main range of variation of extant mysticete species. This is consistent with the model elaborated by Goldbogen et al. (2019) on the hypothesized metabolic path able to drive the evolution of gigantism in mysticetes suggesting that gigantic body size (i.e., TL >



558 20 m) should be considered as an exceptional output of an evolutionary lineage rather than the  
1  
559 normal *status quo*.  
3  
4  
560 Interestingly, our data suggest that the temperature decrease of the Pleistocene did not impact  
6  
561 mysticete biology in only one sense (i.e., evolution of gigantic TL values); rather, during  
8  
562 Pleistocene, we observe an increase in the TL range suggesting evolution of different ecological  
10  
11  
1563 strategies and, possibly, occupation of more ecological niches. This is particularly evident in the  
13  
14  
1564 rorquals of the North Atlantic that have different alimentary specializations (see reviews in Barros  
15  
16  
1565 and Clarke, 2002; Kawamura, 1980) and in the geographic differentiation of right and bowhead  
18  
19  
1566 whales. More detailed analysis of the morphological changes occurred in the Plio-Pleistocene are  
20  
21  
22  
23  
24  
2567 necessary to test this hypothesis but this is beyond the scope of the present paper.  
26  
27  
28  
29  
30  
31  
32  
33  
34  
35  
36  
37  
38  
39  
40  
41  
42  
43  
44  
45  
46  
47  
48  
49  
50  
51  
52  
53  
54  
55  
56  
57  
58  
59  
60  
61  
62  
63  
64  
65

568 Based on the operational definition of gigantism, we observe that gigantic size occur only in  
569 Balaenopteridae and Balaenidae. All the other mysticete taxa were small-to-middle sized  
(Supplementary Fig. S3). The first increase in body size range is contemporaneous with the early  
appearance of the basal thalassotherian taxa in the early Langhian following a period characterized  
by high rate of morphological change (Fig. S1 in Supplementary File 1). A slight increase in mean  
TL is observed in Tortonian (mean TL is *c.* 5 m) and Messinian (mean TL is *c.* 7 m) (Fig. 10).  
Subsequently, a slight change in mean TL is observed in the early Pliocene (mean TL is *c.* 6 m); an  
abrupt increase in the mean TL is observed starting from the earliest Pleistocene (mean TL is *c.* 10  
m). The smallest mysticetes (TL < 5 m) disappear from the fossil record starting from the  
Calabrian, in the middle Pleistocene.

Family trends are shown in Figs S1-S3 (Supplementary File 1). The graphs show that different  
trends occurred in different families. Among the earliest mysticetes, in the time interval between 28  
and 25 Ma, we observe that the eomysticetids and Aetiocetidae increased their TL, although  
*Maiabalaena*-like taxa decreased TL values suggesting that a process of niche partitioning possibly  
took place. In the time interval between 16 and 10 Ma, we observe an early TL increase in the basal  
thalassotherian taxa but a subsequent drop in TL values around 12 Ma when the Cetotheriidae

584 started increasing TL values. The same observation is made for the time interval between 9 and 2  
1  
585 Ma when the TL reduction in the Cetotheriidae occurred with the TL increase occurring in the  
3  
4  
586 Balaenopteridae. The last cetotheriids (*Herpetocetus* sp.; Boessenecker, 2013) had the smallest size  
6  
587 of all Cetotheriidae and were living side to side with large balaenopterids (Fig. S2).  
8  
9  
588 The maximum mysticete diversity was attained during the middle Miocene and is characterized by  
10  
11  
589 an expansion in the body size range that included small-, medium-, and large-sized species (Fig.  
13  
14  
590 S1); this pattern is observed up to the early Pliocene when small and medium-sized mysticetes are  
15  
16  
591 the only ones present in the fossil record but large- and gigantic-sized species are absent. A new  
18  
19  
592 expansion in TL range with evolution of small-, medium-, large-, and gigantic-sized species starts  
20  
21  
593 from the beginning of Pleistocene and leads to the present time (Fig. S2).  
22  
23  
594 We reconstructed the most likely size at the ancestral nodes of the phylogeny shown in Fig. 2 using  
25  
26  
595 the maximum likelihood algorithm of MESQUITE, which are shown in Fig. 11. We observe that  
27  
28  
596 most of the TL values for extinct mysticetes fall in the small-sized category; medium, large and  
30  
31  
597 gigantic sizes evolved independently in several lineages. The large size of the Tortonian  
32  
33  
598 balaenopterid MuMAB 240508 is interpreted as an early and independent evolution of large body  
35  
36  
599 size in an archaic, early balaenopterid. Interestingly, in the time interval comprised between  
37  
38  
600 Langhian and Tortonian, a number of mysticetes evolved a medium size; these include *Uranocetus*  
40  
41  
601 *gramensis*, *Pelocetus calvertensis*, *Archaeschrictius ruggieroi*, *Norrisanima miocaena* and  
42  
43  
602 *Plesiobalaenoptera quarantellii*. Interestingly, eschrichtiids appear to have been medium-sized  
45  
46  
603 since their origin. A trend toward increasing TL values is observed in the Balaenopteridae starting  
47  
48  
604 from the Tortonian (*Norrisanima miocaena*) up to today, although a trend in miniaturization that  
49  
50  
605 involved the origin of the extant minke whale (*Balaenoptera acutorostrata*) can be also observed.  
52  
53  
606 This is not surprising in the light of a hypothesis of a niche partitioning process during the last  
54  
55  
607 million years (Fig. 11). Gigantism is never observed as the unambiguous ancestral state for a  
57  
58  
608 mysticete clade even though a TL increase represents an ancestral character of a single rorqual  
59  
60  
609 clade (the one leading to the extant species of *Balaenoptera* and *Megaptera*).  
61

610  
1  
611  
3  
4  
612  
6  
613  
8  
9  
614  
10  
11  
615  
13  
14  
616  
15  
16  
617  
18  
618  
20  
21  
619  
23  
24  
25  
620  
26  
621  
27  
28  
622  
30  
31  
623  
32  
33  
624  
35  
36  
625  
37  
38  
626  
40  
41  
627  
42  
43  
628  
44  
45  
629  
47  
48  
630  
49  
50  
631  
52  
53  
632  
54  
55  
633  
57  
58  
634  
59  
60  
635  
62  
63  
64  
65

### 3.5. Relationships to Cenozoic global change

The relationships between the patterns of body size and morphological evolution of mysticete cetaceans and Cenozoic global events, reported in Figs. 12-14, are discussed herein.

#### 3.5.1. $\alpha$ 1-3 events

The  $\alpha$ 1-3 events of mysticete diversification occurred around the Eocene/Oligocene boundary (ca. 39 to 28 Ma). During the E/O transition the climate changed from greenhouse to icehouse conditions, with the establishment of the first Antarctic glacial cover about 37 Ma (Zachos et al., 2001; Fig. 12). The global average temperatures dropped from ca. 24°C (Middle Eocene Thermal Maximum; Scotese et al., 2022; Fig. 12) to ca. 15°C (major drop of the Late Eocene-Oligocene Cooling; Scotese et al., 2022; Fig. 12). At the same time, remarkable turnovers occurred in terrestrial ecosystems, where grasses started to spread, probably favored by a concurrent intensification of the fire regime (Strömberg & Staver, 2022; Fig. 13). Major tectonic events during this period include the onset of the Alpine-Himalayan orogeny (Cermeño et al., 2015; Fig. 13), as well as the opening of the Drake and Tasmanian passages, which initiated the isolation of the Antarctic landmass and the establishment of the Proto-Antarctic Circumpolar Current (Potter & Szatmari, 2009, 2015; Sarkar et al., 2019; Fig. 13). Significant volcanic activity is recorded in Africa, associated with the Hoggar volcanism, the eruption of Ethiopian traps and the initial Red Sea and East African rifting (Rognon et al., 1983; Ait-Hamou et al., 2000; Couvreur et al., 2020; Boone et al., 2021; Fig. 13), in America (Basin and Range and Great Basin volcanism; Sternai et al., 2021; Fig. 13), and in Iceland, with a marked increase of the magmatic flux (Døssing et al., 2016; Fig. 13). Although the sediment yield decreased during the  $\alpha$ 1-3 events, the occurrence of an active weathering in continental settings is suggested by Sr isotopes, which show a slight but continuous increase from the  $\alpha$ 1 event onward, and by the dissolved Si flux, which peaked around

636 the  $\alpha_3$  event (Fig. 12). Intriguingly, the  $\alpha_2$  event coincided with the most significant  
1  
637 phosphogenetic event recorded in the Cenozoic (e.g., Hyeong et al., 2013). Diatom productivity  
3  
638 raised shortly after the  $\alpha_2$  event, as well as diatom diversity, both accompanied by a positive peak  
4  
639 in  $\delta^{13}\text{C}$  (Zachos et al., 2001; Renaudie, 2016; Fig. 14). Although during this period the  
6  
640 diatomaceous production was mostly focused in the South Atlantic (Renaudie, 2016; Fig. 14), an  
8  
641 explosive diversification and abundance increase of *Chaetoceros* resting spores is also recorded in  
10  
642 the North Atlantic during the  $\alpha_1$  and  $\alpha_2$  events (Suto, 2006; Fig. 14), and a prolonged period of  
12  
643 opal accumulation also occurred in the Southern Pacific (Sarkar et al., 2019; Fig. 14), in  
14  
644 coincidence with the initial establishment of the Northern Component Water and of the Proto-  
16  
645 Antarctic Circumpolar Current (Steinhorsdottir et al., 2021; Fig. 14). The E/O transition also  
18  
646 recorded the rise of basal lanternfishes, which started to colonize the mesopelagic environment,  
20  
647 slightly increasing their mean sizes at least from the  $\alpha_1$  to  $\alpha_2$  event (Schwarzhan & Carnevale,  
22  
2021; Fig. 14).

### 649 3.5.2. $\beta$ event

650  
651  
652 The  $\beta$  event of mysticete diversification coincided with another drop in the global temperatures  
653 (Fig. 12). On lands, grasslands expansion continued at the expense of forests, with the appearance  
654 of the first grass-dominated ecosystems in North America (Strömberg & Staver, 2022; Fig. 13). The  
655 main tectonic and erosional events during this period were the closure of the Indonesian gateways,  
656 the Southern Cordillera uplift and a generalized uplift of Northern Europe and for a less extent of  
657 the Asian region, this latter favoring an increased siliciclastic deposition in the Mekong and Red  
658 River basins (Potter & Szatmari, 2009, 2015; Cather et al., 2012; Ollier & Pain, 2019; Fig. 12).  
659 Volcanism was mostly associated to the Great Basin Ignimbrites (Sternai et al., 2021; Fig. 13).  
660 Sediment input to the oceans was significantly higher than during the previous  $\alpha$  events (Sternai et  
661 al., 2021) as well as Sr isotopes, although the Si flux from continents was less pronounced than

662 during the  $\alpha$ -3 event (Renaudie, 2016; Fig. 12). Phosphogenesis persisted at rather high rates  
1  
663 (Hyeong et al., 2013; Fig. 14). Diatom abundance was high at the beginning of this event, while  
3  
664 diatom diversity increased at the end (Renaudie, 2019; Fig. 14). Remarkably, the  $\beta$  event coincided  
6  
665 with another  $\delta^{13}\text{C}$  rise, the so-called Oligocene-Miocene Carbon Maximum (Zachos et al., 2001;  
8  
666 Steinthorsdottir et al., 2021; Fig. 12), with the first significant event of opal deposition in the  
10  
667 Southern Ocean and in another peak of diversification of *Chaetoceros* resting spores in the North  
13  
668 Atlantic (Suto, 2006; Fig. 14). The  $\beta$  event also recorded an increase of diversity of lanternfishes  
15  
669 (especially of the very abundant genera *Diaphus* and *Lobianchia*), although slightly smaller in size  
18  
670 than before (Schwarzahans & Carnevale, 2021; Fig. 14).  
20

21  
671

### 672 3.5.3. $\gamma$ event

25  
673

28  
674 This event partly overlapped the Early Miocene Cooling Interval (Scotese et al., 2022; Fig. 12).  
30  
675 Noteworthy, deserts started to expand in the Asian continental interior, as witnessed by the first  
32  
676 remarkable spike of aeolian quartz in the detrital contribution to Pacific Ocean (Guo et al., 2002;  
35  
677 Zheng et al., 2016; Fig. 12). During this period, the global rates of ridge spreading reached a  
37  
678 minimum (Potter & Szatmari, 2009; Fig. 13), although Red Sea rifting went on (Boone et al., 2021;  
40  
679 Fig. 13), the Hoggar volcanism increased (Rognon et al., 1983; Ait-Hamou et al., 2000; Fig. 13),  
42  
680 uplift occurred in Europe (Pyrenees, Lake District, Peninnes; Ollier & Pain, 2019), and sediment  
45  
681 yield and Sr isotopes continued to increase (Sternai et al., 2021; Renaudie, 2016; Fig. 12).  
47  
682 Dissolved Si flux remained rather stable (although they may have decreased if considering the clay-  
49  
683 based inference instead of the Li isotopes; Cermeño et al., 2015). According to Renaudie (2016),  
52  
684 the early Miocene diatom productivity was rather scarce. Some new loci of diatomaceous  
54  
685 deposition started to occur at the mid latitudes, probably in response to the onset of coastal  
57  
686 upwelling cells (Renaudie, 2016; Fig. 14). Phosphogenesis persisted up to the initial part of this  
59  
687 event, then drastically dropped (Hyeong et al., 2013; Fig. 14). Lanternfishes diversity expanded,  
62  
63  
64  
65

688 and their size increased again after the slight decrease occurred during the  $\beta$  event (Schwarzhan &  
1 Carnevale, 2021; Fig. 14).  
689

3  
4  
690

6  
691 *3.5.4. 1, 2 and 3 events*  
8

9  
692

11  
693 From the middle Miocene onward, remarkable climatic, tectonic, ecological and oceanographic  
13  
14  
694 transitions occurred. Following the Mid-Miocene Thermal Maximum, global temperatures and sea  
15  
16  
695 level started to drop again, inaugurating the Late Miocene Cooling Interval and the Messinian  
18  
19  
696 Glaciations, a prelude to the subsequent Pleistocene glaciations (Haq et al., 1987; Scotese et al.,  
20  
21  
697 2022; Fig. 12). Ice-sheet appeared in the Northern Hemisphere (Zachos et al., 2001; Fig. 12).

23  
24  
698 Increasing aridity led to the full establishment of flammable, grass-dominated ecosystems populated  
25  
26  
699 by hypsodont grazers (Strömberg & Staver, 2022; Fig. 13). Desert expanded in Southern and  
28  
29  
700 Central-North Africa and South America, and the dust contribution to detrital fraction significantly  
30  
31  
701 increased (Senut et al., 2009; Jordan et al., 2014; Schuster et al., 2006; Zheng et al., 2016; Fig. 13).

33  
34  
702 Tectonic activity (notably the Andean and Himalayan uplift; the closure of the Mediterranean to  
35  
36  
703 Atlantic gateways leading to the Messinian salinity crisis; Fig. 14), erosional processes (e.g.,  
37  
38  
704 increased siliciclastic influx to North American, Indian and Asian basins) and volcanism (e.g.,  
40

41  
705 Columbia River Basalts; Fig. 14) were globally enhanced, likely in response to the reactivation of  
42  
43  
706 the African and Pacific superplumes (Potter & Szatmari, 2009, 2015; Fig. 14). A significant  
45  
46  
707 increase of sediment yield, Sr isotopes and dissolved Si flux occurred, particularly marked from the  
47  
48  
708 middle to late Miocene (Sternai et al., 2021; Renaudie, 2016; Fig. 12). Both diatom abundance and  
49

50  
51  
709 diversification underwent significant peaks, decreasing after the early Pliocene, especially at the  
52  
53  
710 low-to-mid latitudes (Renaudie, 2016; Fig. 14). With the firm establishment of the North Atlantic  
54

55  
56  
711 Deep Water in the middle Miocene, the thermohaline circulation assumed the present-day  
57  
58  
712 configuration. This led to the so-called ‘silica switch’ from the Atlantic to the Pacific, i.e. a general  
59  
60  
713 nutrient impoverishment of the Atlantic Ocean and the shift of the main loci of opal deposition  
62

714 along the Pacific upwelling cells, strengthened by the increased pole-to-equator thermal gradient  
1  
715 (Keller & Barron, 1983; Barron, 2022; Fig. 14). Consequently, the enhanced shuttling of organic  
3  
716 matter to the seafloor favored new community of sea-floor inhabitants, like benthic foraminifera  
4  
6  
717 adapted to exploit organic-rich substrates (Steinthorsdottir et al., 2021). Organic matter  
8  
718 accumulation was particularly favored in semi-enclosed basins such as the Mediterranean, where  
9  
10  
11  
12  
13  
14  
15  
16  
17  
18  
19  
20  
21  
22  
23  
24  
25  
26  
27  
28  
29  
30  
31  
32  
33  
34  
35  
36  
37  
38  
39  
40  
41  
42  
43  
44  
45  
46  
47  
48  
49  
50

## 51 4. Discussion

### 52 4.1. Phylogenetic relationships of mysticetes

53 The morphological dataset used in the present paper is a modified version of previously used  
54  
55  
56  
57  
58  
59  
60  
61  
62  
63  
64  
65

740 inclusion of taxa and characters to resolve the relationships of basal mysticete taxa. We found a  
1  
741 monophyletic clade including *Llanocetus*, *Toipahautea*, *Maiabalaena*, *Mystacodon*, and  
3  
4  
742 *Coronodon*, and we found that Mammalodontidae (including *Mammalodon* and *Janjucetus*) is the  
6  
743 most basal mysticete clade. These results differ from other works published recent years by  
8  
9  
744 different research groups. For example, Geisler et al. (2017), in a phylogenetic analysis of  
10  
11  
745 *Coronodon*, found that Janjucetidae and Mammalodontidae formed a monophyletic clade and that  
13  
14  
746 *Llanocetus* is the sister group of Chaeomysticeti. These results were confirmed in large part by  
15  
16  
747 Lambert et al. (2017) who found that *Mystacodon* was the most basal mysticete instead of  
18  
19  
748 *Coronodon*. Interestingly, both the monophyly of Mammalodontidae and Aetiocetidae, and the  
20  
21  
749 sister group relationship of *Llanocetus* and Chaeomysticeti resulted from the analysis of Marx et al.  
23  
24  
750 (2015) on *Fucaia buelli*.  
25  
26  
751 A noticeable difference is observed in the work by Fordyce & Marx (2018) who found that a clade  
27  
28  
752 formed by *Llanocetus* and *Mystacodon* represents the most basal mysticete clade with a more  
30  
31  
753 advanced position of Mammalodontidae in the tree. In this work, the monophyly of  
32  
33  
754 Mammalodontidae and Aetiocetide is not supported and the exclusion of *Morawanocetus* from  
35  
36  
755 Aetiocetidae questions the monophyly of this group.  
37  
38  
756 Cisneros et al. (2018) maintained the monophyly of Mammalodontidae and Aetiocetidae but, in that  
40  
41  
757 work, this clade is the most basal mysticete clade and found that *Llanocetus* was the sister group of  
42  
43  
758 the stem Chaeomysticete taxa *Sitsqwayk* and *Tlaxcallicetus*.  
45  
46  
759 Muizon et al. (2019) found another different solution in which *Mystacodon* is the most basal  
47  
48  
760 mysticete that is the sister group of a sequence of taxa formed by, respectively, *Coronodon*,  
49  
50  
761 *Llanocetus* and Aetiocetidae, being the last the sister group of Chaeomysticeti. Tsai & Fordyce  
52  
53  
762 (2018) found a monophyletic clade including *Coronodon*, Mammalodontidae and Aetiocetidae that  
54  
55  
763 was basal in their phylogeny of the mysticetes. They supported a sister group relationships between  
57  
58  
764 *Llanocetus* and Chaeomysticeti with *Toipahautea* nested well within basal chaeomysticetes. This  
59  
60  
765 solution represented a significant change from a previous paper published by Tsai & Fordyce  
62  
63  
64  
65



766 (2016) in which two different topologies were proposed depending on the search strategy of the  
1  
767 most parsimonious tree: (a) a search based on unordered and unweighted characters resulted in  
3  
4  
768 *Llanocetus* being the most basal mysticete and the clade formed by Mammalodontidae and  
6  
769 Aetiocetidae was the sister group of Chaemysticeti, (b) a search based on weighted characters  
8  
770 resulted in a clade formed by Mammalodontidae, Aetiocetidae and *Coronodon* as being the most  
10  
11  
1771 basal mysticete group and in *Llanocetus* being the sister group of Chaemysticeti.  
13  
14  
1772 This review shows that there are different opinions about the early evolution of mysticetes among  
15  
16  
1773 students. Particularly debated are the relationships of *Llanocetus*, Aetiocetidae and  
18  
19  
1774 Mammalodontidae and their relationships with Chaemysticeti. Our results highlight the possibility  
20  
21  
2775 that a single clade of early-diverging, toothed mysticetes diversified after its divergence from the  
23  
24  
2776 ancestor it shared with Aetiocetidae, acknowledge the basal position of Mammalodontidae  
25  
26  
2777 (according to, e.g., Bisconti & Carnevale, 2022) and suggests that Aetiocetidae was a primitive,  
28  
2778 well-diversified taxon that did not share a direct common ancestor with Chaemysticeti.  
30  
31  
32  
33  
3780 *4.2. Mysticete chronology in context*  
35  
36  
3781 Most of the past attempts to infer divergence estimates for the main mysticete clades relied on some  
37  
38  
3782 kind of molecular clock or total evidence analyses (Árnason et al., 2018; Marx and Fordyce, 2015;  
40  
41  
4783 Geisler et al., 2011; McGowen et al., 2009; Steeman et al., 2009; Sasaki et al., 2005). This is the  
42  
43  
4784 first attempt to provide divergence dates that are inferred based on occurrence data from  
45  
46  
4785 fossiliferous localities all over the world. Our results are partially consistent with those provided by  
47  
48  
4786 earlier studies as shown in Fig. S4 (Supplementary File 1). In particular, we observe that the dates  
49  
50  
5787 proposed by previous studies for mysticete divergence range from *c.* 39 to *c.* 28 Ma and our  
52  
53  
5788 hypothesis falls within the lower part of this range (*c.* 38 Ma). We believe that an older divergence  
54  
55  
5789 date for mysticetes is in better agreement with the stratigraphic ages of earliest, toothed-mysticetes  
57  
58  
5790 such as *Llanocetus* and *Mystacodon*; these species date back to about 33 Ma, thereby excluding  
59  
60  
6791 younger divergence dates for mysticetes (such as *c.* 28 Ma as proposed by McGowen et al., 2009).

792 The age of divergence of the Chaecomysticeti ranges between *c.* 36 and *c.* 31 Ma with our result  
1  
793 placed in around the middle part of this interval (*c.* 34 Ma; Fig. S4). All of these proposed dates  
2  
794 suggest that the origin of baleen-assisted feeding in mysticetes evolved fast after the origin of the  
3  
795 group. Based on our morphological dataset, a limited number of morphological transformations  
4  
796 occurred at the transition to the Chaecomysticeti (Fig. 9; see also Bisconti and Carnevale, 2022), thus  
5  
797 supporting the hypothesis that a limited amount of time is expected to be necessary to complete the  
6  
798 structuring of the specialized character states diagnostic for the Chaecomysticeti.  
7  
799 The proposed estimated dates for the divergence of Balaenomorpha range from *c.* 35 and *c.* 23 Ma;  
8  
800 our analysis resulted in a divergence date at *c.* 23 Ma (close to the Oligocene-Miocene boundary)  
9  
801 (Fig. S4). Actually, there are no known balaenomorph mysticetes in the fossil record before the  
10  
802 earliest Miocene. Even though this should be due to collection bias, the only two known taxa close  
11  
803 to the Balaenomorpha (i.e., *Sitsqwayk cornishorum* and *Horopeta umarere*) show plesiomorphic  
12  
804 character states supporting their exclusion from the Balaenomorpha. We interpret both *Sitsqwayk*  
13  
805 and *Horopeta* as stem-Balaenomorpha. These two taxa are the only ones breaking the long branch  
14  
806 that links the common ancestor of Balaenomorpha to the non-balaenomorph mysticetes, revealing  
15  
807 that our knowledge of the evolution of stem-balaenomorph mysticetes is not fully adequate. Marx et  
16  
808 al. (2019) observed this phenomenon and called it a ‘dark age’ of mysticete evolution but limited  
17  
809 the stratigraphic extension of this interval to a few million years before and after the Oligocene-  
18  
810 Miocene boundary and linked it to the faunal turnover that occurred when archaic mysticetes  
19  
811 (including toothed mysticetes and earliest chaecomysticetes) went extinct and being replaced by  
20  
812 balaenomorph mysticetes. We extend the cryptic period characterized by the absence of knowledge  
21  
813 about the origin of Balaenomorpha to a time interval of *c.* 13 million years from *c.* 33 to *c.* 20 Ma.  
22  
814 In this interval, the toothed mysticetes and early chaecomysticetes went extinct and the set of  
23  
815 synapomorphies diagnostic of Balaenomorpha was assembled. We will discuss about biotic and  
24  
816 abiotic forcing of this event later.  
25  
26  
27  
28  
29  
30  
31  
32  
33  
34  
35  
36  
37  
38  
39  
40  
41  
42  
43  
44  
45  
46  
47  
48  
49  
50  
51  
52  
53  
54  
55  
56  
57  
58  
59  
60  
61  
62  
63  
64  
65

817 Based on literature, there is an interval of *c.* 16 million years between the older and the younger  
1  
818 proposed divergence date of the crown Balaenidae. McGowen et al. (2009) provided a range  
3  
819 included between 9.6 and 2.6 Ma that is at odd with fossil evidence suggesting that crown balaenids  
4  
6  
820 were already broadly present in European, North American and Japanese localities in the latest  
8  
9  
821 Miocene, thereby excluding the younger part of the proposed time interval. Sasaki et al. (2005)  
10  
11  
822 proposed an age of  $17.1 \pm 3.5$  Ma; the older part of this range is in good agreement with the presence  
13  
14  
823 of an early balaenoid from the early Miocene of Argentina (*Morenocetus parvus*; Buono et al.,  
15  
16  
824 2017). Our proposed divergence date places the origin of crown Balaenidae *c.* 7.3 Ma, which is in  
18  
19  
825 agreement with both our interpretation of *Morenocetus* as more closely related to *Caperea* than to  
20  
21  
826 Balaenidae and the balaenid fossil record (Bisconti et al., 2021a; Churchill et al., 2011).  
22  
23  
827 Previous hypotheses placed the divergence date of Balaenopteroidea in a range comprised between  
25  
26  
828 *c.* 18 and *c.* 11 Ma. Our result is more consistent with most of the balaenopterid fossil record and  
27  
28  
829 suggests that the balaenopteroids originated around 14 Ma. The taxonomic status and stratigraphic  
30  
31  
830 age of the early Miocene *Protororquaus dyticus*, a possible balaenopterid from the early Miocene of  
32  
33  
831 Argentina (see Bisconti and Bosselaers, 2021; Cabrera, 1926), is critical in this respect, as it could  
35  
36  
832 push back the origin of Balaenopteroidea by several million years, supporting an early Miocene  
37  
38  
833 origin of this group as suggested by Steeman et al. (2009).  
40

### 834 42 43 835 *4.3. Main mysticete evolutionary events and their relation to global dynamics*

836 *4.3.1. Origin and early evolution.* Our results suggest that the origin of mysticetes occurred *c.*38  
47  
48  
837 Ma. We were able to detect only a few factors fully concomitant with this event: (1) the opening of  
49  
50  
838 the Drake Passage, (2) explosive increase of *Chaetoceros* spores in the sedimentary record, and (3)  
52  
53  
839 increased Basin and Range volcanism (Figs 13, 14). The increased abundance of *Chaetoceros*  
54  
55  
840 spores suggests increased availability of food resources for pelagic fishes and macrozooplankton  
57  
58  
841 able to sustain populations of early, toothed-mysticetes. The opening of the Drake Strait between  
59  
60  
842 today Cape Horn and the South Shetland Islands and Antarctica was proposed long ago as a

843 possible trigger for the origin of mysticetes because this event activated the Circum-Antarctic  
1  
844 Current that provides massive nutrient input to the planktonic communities of the Southern  
3  
845 Hemisphere (Fordyce, 1977, 1980). At the time, this interpretation was based on the occurrence of  
4  
846 the earliest mysticete fossils in New Zealand. It is not to be excluded that the nutrient injection by  
6  
847 the volcanic activity and the early onset of the Circum-Antarctic Current acted as co-promoting  
8  
10  
11 factors in the setting of oceanic trophic chains with a remarkable increase of food availability. In  
12  
13 this environmental context, the evolution of a novel predatory bauplan among cetaceans, that  
14  
15 characteristic of early mysticetes, allowed the exploitation of newly developed trophic resources  
16  
18 apparently without strong selective regimes. However, our work shows that the origin of the earliest  
19  
20 mysticetes resulted from a period with high rate of morphological change (Fig. 9) that may be the  
21  
22 result of directional selection. It is difficult to determine which of these two factors promoted the  
23  
24 fast process leading to the assembly of the mysticete body plan (Bisconti and Carnevale 2022) even  
25  
26 though the environmental context outlined above suggests that selection should have played a minor  
27  
28 role in this process. Directional selection would result from loss of resources triggering strong  
29  
30 competition but this does not seem the case for the origin of mysticetes, which occurred at a time of  
31  
32 increased food resources.  
33  
34  
35 Based on our results, the origin of chaemysticetes ( $\alpha_2$  event) occurred around 28 Ma. The main  
36  
37 factor that can be correlated with this event is a large phosphogenetic event (Fig. 14). Additional  
38  
39 events are shown in Fig. 13 that could correlate with the  $\alpha_1$  event; these include the final phases of  
40  
41 the opening of the Drake Passage, the opening of the Tasmania-Antarctica Passage and a number of  
42  
43 volcanic events. The recent discovery of aetiocetid mysticetes in the North Pacific and of  
44  
45 eomysticetid baleen whales in North and South Pacific, North Atlantic and Tethys suggests that one  
46  
47 or more global factors promoted the origin and early diffusion of chaemysticetes in these oceanic  
48  
49 basins (Bisconti 2010). It cannot be excluded that the massive deposition of phosphorites occurring  
50  
51 in the early Oligocene was related to the massive blooms of fish and plankton populations at  
52  
53 worldwide scale. Large availability of food resources may have set a comfortable environmental  
54  
55  
56  
57  
58  
59  
60  
61  
62  
63  
64  
65

869 context in which even a low rate of morphological change (Fig. 9) promoted the assembly of the  
1  
870 chaeomysticete body plan characterized by the presence of elongated rostra, baleen for filter-  
3  
871 feeding, loss of radial crest from the radius and change in orientation of the olecranon process of the  
6  
872 ulna (Bisconti and Carnevale 2022); these characters affect the methods used by mysticetes to  
8  
873 access food resources through direct catch and swimming behaviors.  
10

11  
1874 Interestingly, there is no apparent competition dynamics in the curve depicting the ‘evolutionary  
13  
14  
875 faunas’ around 34 Ma but, rather, earliest chaeomysticetes and toothed mysticetes coexisted without  
15  
16  
1876 apparent interference. This observation suggests that there was no niche overlap and, therefore, the  
18  
19  
877 earliest baleen-bearing mysticetes exploited different trophic sources from those exploited by  
20  
21  
878 toothed mysticetes. An accurate analysis of the feeding biomechanics of toothed- and baleen-  
23  
24  
879 bearing mysticetes would be highly desirable to test this hypothesis. Tsai and Kohno (2016) and  
25  
26  
880 Tsai and Ando (2016) suggested that a process of niche partitioning took place during the time  
27  
28  
881 interval of existence of the Aetiocetidae as they were able to show that there was an observable  
30  
31  
882 interval of size variation in this group at the end of the Oligocene.  
32

33  
883 The origin of chaeomysticetes should be regarded as an evolutionary process leading a group to  
35  
36  
884 invade a new trophic niche by means of novel morphological and functional characteristics. This  
37  
38  
885 process occurred through low rate of morphological change within an environmental context rich in  
40  
41  
886 food resources as testified by massive global deposition of phosphorites, increased diatom diversity  
42  
43  
887 and high values of  $\delta^{13}\text{C}$  with respect to the previous few million years and, most notably, with  
45  
46  
888 apparent lack of competition between toothed- and early baleen-bearing mysticete species.  
47

48  
889  
50  
890 *4.3.2. Miocene diversification events.* Analysis of clade diversity suggests that the origin of crown-  
52  
53  
891 mysticetes (Balaenomorpha) occurred at the very end of the Chattian (latest Oligocene), at a time  
54  
55  
892 when toothed- and early baleen-bearing mysticetes underwent a worldwide, massive extinction  
57  
58  
893 process without a corresponding replacement events (Figs 5, 6). This cryptic ‘dark age’ of mysticete  
59  
60  
894 evolution was also documented by Marx et al. (2019) who suggested that differential survival of  
62  
63  
64  
65

895 mysticete species depended on the habitat they inhabited with oceanic species being more likely to  
1  
896 survive than more coastal species. Marx et al. (2019) observed also a drop in diversity in some  
3  
4  
897 odontocete groups, with the extinction of certain groups such as the Xenorophiidae, and suggested  
5  
6  
898 that the sea level rise, between the latest Oligocene and the end of the Aquitanian (Fig. 9), was  
8  
9  
899 responsible for the loss of the coastal niches necessary to sustain whales living more inshore. Both  
10  
11  
900 origination and extinction rates were null in this period thus suggesting that a sampling bias could  
13  
14  
901 affect our knowledge of mysticete diversity. Further exploration of latest Oligocene-to-Early  
15  
16  
902 Miocene fossiliferous horizons at global scale will confirm or dismantle this hypothesis but,  
18  
19  
903 currently, we must assume that only a limited number of mysticetes survived the extinctions at the  
20  
21  
904 end of the Oligocene and gave rise to Balaenomorpha.  
22  
23  
905 The analysis of the rates of morphological change showed that only a few transformations occurred  
25  
26  
906 between the common ancestor of Chaeomysticeti and *Horopeta umarere*, one of the earliest stem-  
27  
28  
907 balaenomorph mysticetes, but a high number of morphological changes occurred from the common  
30  
31  
908 ancestor of *Horopeta* + Balaenomorpha and the common ancestor of Balaenomorpha. This suggests  
32  
33  
909 that the early steps leading to the novel architectures of stem-balaenomorph mysticetes were  
35  
36  
910 relatively few but a high number of transformation events (Fig. 9) were necessary for the complete  
37  
38  
911 assembly of the balaenomorph body plan. These changes occurred in less than 4.5 Ma suggesting  
40  
41  
912 the existence of a directional selection active during the earliest Oligocene-to-Early Miocene.  
42  
43  
913 Apparently, there was not a competitive dynamics underlying this phase as the documented  
44  
45  
914 diversity of balaenomorph mysticetes (as documented by both fossil record and clade diversity)  
47  
48  
915 remained low until the end of the Aquitanian, *c.* 20 Ma (Fig. 9). By that epoch, balaenomorph  
49  
50  
916 mysticetes underwent an explosive radiation through the fast divergence of Balaenoidea and  
52  
53  
917 Thalassotherii, two clades characterized by profoundly different trophic strategies and  
54  
55  
918 biomechanics.  
56  
57  
919 The  $\beta$  event, corresponding to the origin and early differentiation of Balaenomorpha, occurred after  
59  
60  
920 a period of temperature instability during which stem-balaenomorph mysticetes began to appear in  
62  
63  
64  
65

921 the oceans. A peak in origination rate is recorded around 20 Ma based on clade diversity, suggesting  
1  
922 that most of the early diversification of Balaenomorpha occurred without increased extinction rate  
3  
4  
923 (Fig. 6). For the first time, it is possible to observe an increase in body size (Fig. 10) suggesting that  
6  
924 the differentiation between alternative filter feeding mechanisms was paralleled by a niche  
8  
9  
925 partitioning process that generated a wider body size range among mysticetes. The end of one of the  
10  
11  
926 main phosphogenetic episodes of the Cenozoic occurred just about 20 Ma (Fig. 14) at a time when  
13  
14  
927 the major clades of Balaenomorpha were just established. We found that a peak in  $\delta^{13}\text{C}$  is recorded  
15  
16  
928 at about 23 Ma that is followed by a slight drop in  $\delta^{13}\text{C}$  suggesting a decrease of the primary  
18  
19  
929 production in the oceans during the Aquitanian. Based on these observations, we found that two  
20  
21  
930 indicators indicate reduced oceanic productivity in the earliest Miocene suggesting that sharp  
22  
23  
931 selective regimes were active by the end of the Chattian and the end of the Aquitanian. At the end  
25  
26  
932 of this period, the fossil record shows that a process of niche partitioning was completed among  
27  
28  
933 baleen-bearing mysticetes with the establishment of continuous ram feeding Balaenoidea and  
30  
31  
934 intermittent ram feeding stem *Thalassotherii* (Fig. 4). Interestingly, several speciation events  
32  
33  
935 occurred within some of the most representative krill genera, *Euphausia* (Jarman et al. 2000) and  
35  
36  
936 *Nyctiphanes* (D'Amato et al. 2008) between 26 and 16 Ma. The possible diversification of  
37  
38  
937 euphausiids in the late Aquitanian and Burdigalian (Fig. 14) is concomitant with the origin of  
40  
41  
938 intermittent ram feeding mysticetes belonging to basal thalassotherian taxa (Kimura 2002)  
42  
43  
939 suggesting the existence of a possible causal link between these two events. However, there are no  
45  
46  
940 data about the feeding strategies of the predicted stem thalassotherian taxa (not still found in the  
47  
48  
941 fossil record but supposed to have existed by phylogenetic analysis) suggesting that it is not  
49  
50  
942 possible to test this tempting hypothesis at the moment.  
52  
53  
943 We observe a consistent diversification of thalassotherian taxa starting from *c.* 20 Ma (Fig. 5),  
54  
55  
944 approximately at the same time when a massive diversification of oceanic lantern fishes took place.  
57  
58  
945 We dissected this mysticete radiation by realizing curves depicting 'evolutionary faunas' (Fig. 8)  
59  
60  
946 and observe that the overall radiation is constituted by different processes affecting the diversity of  
61  
62  
63  
64  
65



947 the different balaenomorph families. We observe two pulses of diversity increase of basal  
1  
948 thalassotherian taxa at *c.* 20 and *c.* 16 Ma. Then, the diversity of basal thalassotherians decreases  
3  
4  
949 and that of Cetotheriidae increases suggesting a strong competitive regime between these two  
5  
6  
950 families. Currently, the feeding behavior of Cetotheriidae is under debate with two different  
8  
9  
951 hypotheses being supported by different sources of evidence: (a) piscivory supported by the find of  
10  
11  
952 an isolated fish aggregate among the ribs of a Miocene cetotheriid mysticete in Peru (Collareta et al.  
13  
14  
953 2015) and (b) bottom feeding supported by reconstruction of muscular attachments on the dentary  
15  
16  
954 and skull of *Herpetocetus morrowi* (El Adli et al. 2014). Based on the data plotted in Fig. 8 we are  
18  
19  
955 more inclined to suppose that piscivory was shared by both basal thalassotherians and cetotheriids  
20  
21  
956 but, even in this case, a more complete understanding of the feeding biomechanics of these  
22  
23  
957 mysticetes is required to test the hypothesis of competition that we propose to explain the shape of  
25  
26  
958 the curve of the ‘evolutionary faunas’ showing contemporaneous decline in basal thalassotherians  
27  
28  
959 and rise of cetotheriid mysticetes.  
30  
31  
960 Starting from about 14 Ma, we observe an initial decline of the Cetotheriidae contemporaneous to  
32  
33  
961 an initial rise of balaenopterid mysticetes ( $\delta$  event of Fig. 4; Fig. 8). Even in this case, the curve  
35  
36  
962 suggests that a strong competitive regime was acting and balaenopterids resulted more well  
37  
38  
963 equipped to survive this regime. The initial increase of Balaenopteridae is synchronous with an  
40  
41  
964 increase in diatom diversity and with geodynamic events (Fig. 13) suggesting an increased  
42  
43  
965 complexity of the oceanic ecosystems. We suspect that there is a causal link between the peak of  
44  
45  
966 balaenopterid diversity observed between 8 and 9 Ma and the almost contemporaneous peaks in  
47  
48  
967 dissolved Si and detrital input (Fig. 12), suggesting that more nutrients were available for plankton  
49  
50  
968 and, therefore, more food (notably planktic diatoms) was available in the oceanic trophic webs. The  
52  
53  
969 apparent competitive exclusion of Cetotheriidae from access to trophic resources operated by  
54  
55  
970 balaenopterids is probably related to the increased efficiency of food removal performed by the  
57  
58  
971 latter thanks to specialized biomechanical features of the feeding apparatus in the skull and  
59  
60  
972 mandible (Sanderson and Wassersug 1993).

973  
1  
974  
3  
4  
975  
6  
976  
8  
977  
10  
11  
978  
13  
14  
979  
15  
16  
980  
18  
19  
981  
20  
21  
982  
22  
23  
983  
25  
26  
984  
27  
28  
985  
30  
31  
986  
32  
33  
987  
35  
36  
988  
37  
38  
989  
40  
41  
990  
42  
43  
991  
44  
45  
992  
47  
48  
993  
49  
50  
994  
52  
53  
995  
54  
55  
996  
56  
57  
997  
59  
60  
998  
61  
62  
63  
64  
65

#### 4.3.3. Pliocene-to-Recent events.

Even though the Pliocene was characterized by relatively high diversity in mysticetes (mostly due to the increased numbers of balaenid and balaenopterid species), the end of the Pliocene experienced an impoverishment of the mysticete faunas all around the world (Fig. 5). Geodynamic and climatic events approximately synchronous with this pattern include a major temperature drop (starting from *c.* 2.5 Ma) and large-scale oscillations in sea level that may have impacted on the availability of coastal areas for reproduction and feeding of small-sized species (Figs 12, 14). In this time interval, we observe a massive increase in mean body size with the origin and stabilization of gigantic species (*sensu* Bisconti et al. 2021). Earlier occurrences of large-sized and gigantic mysticetes are here regarded as occasional results of isolated phylogenetic lineages.

As a matter of fact, in the last 5 million years we observe the extinction of Cetotheriidae, a pulse in balaenid diversity followed by a drop, and a pulse in balaenopterid diversity followed by a drop after 2.5 Ma. Eschrichtiids (the gray whale) and neobalaenids (the pygmy right whale) maintained a reduced diversity throughout the period. Apparently, the only factors concomitant with the observed pattern are the drop in temperature, eustatic oscillations and the closure of the Central America Seaway with the consequent onset of the Gulf Stream that started to transfer warm waters to the Northern Hemisphere in different way with respect to the late Miocene. These factors were already evidenced by Whitmore (1994) and we support his conclusions with our results. We add the observation that the temperature drop was not only associated to a body size increase but, rather, to a trend toward an expansion in body size range that is still represented among living mysticetes.

Based on our phylogenetic results, for instance, the origin of the minke whale (*Balaenoptera acutorostrata*) corresponds to a miniaturization process from large-sized ancestors (Fig. 11), showing that during the Plio-Pleistocene there was not a single trend in body size change.

Actually, in the late Pliocene and Pleistocene we observe the widest range of body sizes in the whole evolutionary history of mysticetes and this suggests the establishment of a considerable niche

999 partitioning between the species still inhabiting the oceans as body size has long been considered a  
1 straightforward proxy for ecology and niche partitioning (Tsai and Ando, 2016; Damuth and  
1000 2  
3  
4  
1001 5 MacFadden, 1990). This inference is supported by the different alimentary specializations of the  
6  
7  
1002 8 balaenopterid species of the northern hemisphere that feed upon specific prey items (different fish  
9  
1003 9 and krill species; Kawamura 1980), a pattern that is still showing evolutionary trends in the oceans  
10  
11  
1004 12 of today (Gavrilchuk et al. 2014; Ryan et al. 2013).  
13

## 1005 14 15 16 1006 17 **Conclusions**

1007 18 The evolutionary history of baleen whales is punctuated by several diversification events. We  
19  
20  
1008 21 provided a new chronological framework where these events can be included in order to understand  
22  
23  
1009 24 when major origination and extinction pulses occurred and when mysticete body size changed  
25  
26  
1010 27 significantly. We used a newly-generated phylogenetic analysis to infer ancestral sizes at internal  
28  
29  
1011 30 nodes in order to obtain good chronological assessments of all the events. The inference of  
31  
1012 32 chronology depended on (a) an extensive review of the locality of discovery of fossil mysticetes  
33  
34  
1013 35 based on a dataset that included more than 1400 entries and (b) a statistical method based on  
36  
37  
1014 38 sampling intensity of taxa in the localities discussed above. The main chronological results include:  
39  
40  
1015 41 (1) the origin of the mysticetes: *c.* 38 Ma; (2) the origin of the Chaeomysticeti: *c.* 34 Ma; (3) origin  
42  
1016 43 of Balaenomorpha: *c.* 24 Ma; (4) origin of Balaenoidea (pygmy, right and bowhead whales): *c.* 23.3  
44  
1017 45 Ma; (5) origin of Thalassotherii: *c.* 19.9 Ma; (6) origin of Balaenopteroidea (rorquals, humpbacks  
46  
1018 47 and gray whales): *c.* 13.9 Ma.

1019 48 Major origination pulses occurred about 38 Ma, between Bartonian and Priabonian in the Eocene;  
49  
50  
1020 51 about 28 Ma, between Rupelian and Chattian in the Oligocene; and several times since the  
52  
53  
1021 54 Aquitanian. Major extinction pulses occurred between the Rupelian and the Aquitanian (extinction  
55  
56  
1022 57 of toothed mysticetes and earliest chaeomysticetes, including Eomysticetidae), and during the  
58  
1023 58 interval comprised between the Tortonian and the Pliocene. The analysis of ‘evolutionary faunas’  
59  
60  
1024 61 revealed distinct competition regimes between basal thalassotherians and Cetotheriidae and between  
62  
63  
64  
65

1025 Cetotheriidae and Balaenopteridae, suggesting that Cetotheriidae, basal thalassotherians and  
1  
1026 Balaenopteridae occupied similar trophic niches. Apparently, no competition dynamics is observed  
2  
3  
4  
1027 in the Eocene and Oligocene between toothed mysticetes and early chaeomysticetes (mainly formed  
5  
6  
7  
1028 by the Eomysticetidae), supporting the hypothesis that these groups fed in different ways.  
8  
9  
1029 Rates of morphological changes varied throughout mysticete evolution. Higher rates are observed at  
10  
11  
1030 the transition from Archaeocetes to Mysticetes, at the origin of Balaenomorpha, at the origin of  
12  
13  
1031 Thalassotherii, at the origin of Cetotheriidae and at the origin of Balaenopteroidea. Body size  
14  
15  
1032 diversity begins to expand from the Tortonian but the highest rates of body size change occurred in  
16  
17  
1033 the Pleistocene, leading to the origin of gigantic mysticetes still living today.  
18  
19  
20  
1034 There is not a single mechanism explaining all the evolutionary events discussed in this paper. We  
21  
22  
23  
1035 found that different events show relationships with different biotic or abiotic events such as  
24  
25  
1036 geodynamic events (e.g., onset of circum-Antarctic current, wide and strong volcanism, etc.) and  
26  
27  
28  
1037 biological events (e.g., increase in diatom diversity and abundance).  
29  
30  
1038 We provided a wealth of new data and interpretations in terms of chronology and analysis of the  
31  
32  
33  
1039 main drivers in mysticete evolution (extinction/origination rates, rates of size change,  
34  
35  
1040 morphological, taxonomic and clade diversity, major diversification events etc.) and provided a  
36  
37  
38  
1041 global framework to chronologically and biologically interpret the evolution of baleen whales.  
39  
40

## 1042 41 42 43 **Acknowledgments** 44

1044 This work was supported by grants (ex-60% 2021 and 2022) from the Università degli Studi di  
45  
46  
1045 Torino. Many thanks are due to Mark D. Uhen who provided suggestions about statistical literature  
47  
48  
49  
50  
1046 in an early stage of this research. Mark D. Uhen and Toshiyuki Kimura provided accurate reviews  
51  
52  
53  
1047 of this paper greatly improving its scientific content and clarity; we want to warmly thank them for  
54  
55  
56  
1048 their effort. Last but not least, we want to thank Alessandra Negri for her constructive and efficient  
57  
58  
1049 editorial support.  
59  
60  
61  
62  
63  
64  
65

1051  
1  
2  
3  
4  
5  
6  
7  
8  
9  
10  
11  
12  
13  
14  
15  
16  
17  
18  
19  
20  
21  
22  
23  
24  
25  
26  
27  
28  
29  
30  
31  
32  
33  
34  
35  
36  
37  
38  
39  
40  
41  
42  
43  
44  
45  
46  
47  
48  
49  
50  
51  
52  
53  
54  
55  
56  
57  
58  
59  
60  
61  
62  
63  
64  
65

## References

- Aït-Hamou, F., Dautria, J.M., Cantagrel, J.M., Dostal, J., Briquieu, L., 2000. Nouvelles données géochronologiques et isotopiques sur le volcanisme cénozoïque de l’Ahaggar (Sahara algérien): des arguments en faveur d’un panache. *Comptes Rendus Académie Sciences Paris* 330 (12), 829-836. [https://doi.org/10.1016/S1251-8050\(00\)00217-2](https://doi.org/10.1016/S1251-8050(00)00217-2)
- Alroy, J., 2014. Accurate and precise estimates of origination and extinction rates. *Paleobiology* 40, 374–397.
- Árnason, U., Lammers, F., Kumar, V., Nilsson, M.A., Janke A., 2018. Whole-genome sequencing of the blue whale and other rorquals finds signatures for introgressive gene flow. *Sci. Adv.* 4, eaap987.
- Bajpai, S., Gingerich, P.D., 1998. A new Eocene archaeocete (Mammalia, Cetacea) from India and the time of origin of whales. *PNAS* 95, 15464–15468.
- Bannister, J.L., 2009. Baleen whales. In: Perrin, W.F., Würsig, B., Thewissen, J.G.M. (Eds.), *Encyclopedia of Marine Mammals*. Academic Press, San Diego, Pp. 62–72.
- Barron, J.A., 2022. Refined assessment of the paleoceanographic and tectonic influences on the deposition of the Monterey Formation in California. In: Aiello, I., Barron, J.A., Ravelo, C. (eds.), *Understanding the Monterey Formation and similar biosiliceous units across space and time*. Geological Society of America Special Papers. [https://doi.org/10.1130/2022.2556\(06\)](https://doi.org/10.1130/2022.2556(06))
- Barros, N.B., Clarke, M.R., 2002. Diet. In: Perrin, W.F., Würsig, B., Thewissen, J.G.M. (Eds.), *Encyclopedia of Marine Mammals*. Academic Press, San Diego, pp. 323–327.
- Berge, J., Gabrielsen, T.M., Moline, M., Renaud, P.E., 2012. Evolution of the Arctic *Calanus* complex: an Arctic marine avocado? *J. Plankton Res.* 34, 191–195.
- Berta, A., Lanzetti, A., 2020. Feeding in marine mammals: An integration of evolution and ecology through time. *Palaeontol. Electronica* 23, a40.
- Betka, P.M., Thomson, S.N., Sincavage, R., Zoramthara, C., Lalremruatfela, C., Lang, K.A., Steckler, M.S., Bezbaruah, D., Borgohain, P., Seeber, L., 2021. Provenance shift during

- 1077 Neogene Brahmaputra Delta progradation tied to coupled climate and tectonic change in the  
1 Eastern Himalaya. *Geochemistry, Geophysics, Geosystems* 22, e2021GC010026.  
1078  
3  
4  
1079 <https://doi.org/10.1029/2021GC010026>  
6
- 1080 Bianucci, G., Marx, F.G., Collareta, A., Di Stefano, A., Landini, W., Morigi, C., Varola, A., 2019  
8  
9  
1081 Rise of the titans: baleen whales became giants earlier than thought. *Biol. Lett.* 15, 20190175.  
10  
11
- 1082 Bisconti, M., 2007. A new basal balaenopterid from the Early Pliocene of northern Italy.  
13  
14  
1083 *Palaeontology* 50, 1103–1122.  
15
- 1084 Bisconti, M., 2010. Cenozoic environmental changes and evolution of baleen whales. In: Murray,  
18  
19  
1085 C.A. (Ed.), *Whales and dolphins. Behavior, biology and distribution*. Nova Publishers, New  
20  
21  
1086 York, pp. 1–46.  
22  
23
- 1087 Bisconti, M., Bosselaers, M.E.J., 2020. A new balaenopterid species from the Southern North Sea  
25  
26  
1088 Basin informs about phylogeny and taxonomy of *Burtinopsis* and *Protororqualus* (Cetacea,  
27  
28  
1089 Mysticeti, Balaenopteridae). *PeerJ* 8, e9570.  
30
- 1090 Bisconti, M., Carnevale, G., 2022. Skeletal Transformations and the Origin of BaleenWhales  
32  
33  
1091 (Mammalia, Cetacea, Mysticeti): A Study on Evolutionary Patterns. *Diversity*, 14, 221.  
35  
36  
1092 <https://doi.org/10.3390/d14030221>  
37
- 1093 Bisconti, M., Munsterman, D.K., Post, K., 2019. A new balaenopterid whale from the late Miocene  
40  
41  
1094 of the Southern North Sea Basin and the evolution of balaenopterid diversity (Cetacea,  
42  
43  
1095 Mysticeti). *PeerJ* 7, e6915.  
44  
45
- 1096 Bisconti, M., Pellegrino, L., Carnevale, G., 2021. Evolution of gigantism in right and bowhead  
47  
48  
1097 whales (Cetacea: Mysticeti: Balaenidae). *Biol. J. Linn. Soc.* 134, 498–524.  
49  
50
- 1098 Bisconti, M., Raineri, G., Tartarelli, G., Monegatti, P., Carnevale, G., 2022. The periotic of a basal  
52  
53  
1099 balaenopterid from the Tortonian of the Stirone River, northern Italy (Cetacea, Mysticeti,  
54  
55  
1100 Balaenopteridae). *Palaeobiodiv. Palaeoenv.* <https://doi.org/10.1007/s12549-022-00550-2>  
56  
57
- 1101 Boessenecker, R.W., 2013. A new marine vertebrate assemblage from the Late Neogene Purisima  
59  
60  
1102 Formation in Central California, part II: pinnipeds and cetaceans. *Geodiversitas* 35, 815–940.  
61  
62  
63  
64  
65

- 1103 Boone, S.C., Balestrieri, M.L., Kohn, B., 2021. Tectono-thermal evolution of the Red Sea Rift.  
1  
1104 Frontiers in Earth Science (9), 713448. <https://doi.org/10.3389/feart.2021.713448>  
2  
3  
4  
1105 Boscolo-Galazzo, F., Jones, A., Dunkley Jones, T., Crichton, K.A., Wade, B.S., Pearson, P.N.,  
5  
6  
1106 2022. Late Neogene evolution of modern deep-dwelling plankton. Biogeosciences 19, 743-762.  
7  
8  
1107 <https://doi.org/10.5194/bg-19-743-2022>  
9  
10  
11  
1108 Bromham, L., 2019. Six impossible things before breakfast: assumptions, models and belief in  
12  
13  
1109 molecular dating. Trends in Ecol. Evol. 34, 474–484.  
14  
15  
16  
1110 Brusatte, S.L., Montanari, S., Yi, H.-y, Norell, M.A., 2011. Phylogenetic corrections for  
17  
18  
1111 morphological disparity analysis: new methodology and case studies. Paleobiology 37, 1-22.  
19  
20  
21  
1112 Buono, M.R., Fernandez, M.S., Cozzuol, M.A., Cuitiño, J.I., Fitzgerald, E.M.G., 2017. The early  
22  
23  
1113 Miocene balaenid *Morenocetus parvus* from Patagonia (Argentina) and the evolution of right  
24  
25  
1114 whales. PeerJ 5, e4148.  
26  
27  
28  
1115 Cabrera, A., 1926. Cetaceos fosiles del Museo de La Plata. Rev. Mus. la Plata 29, 363–411.  
29  
30  
31  
1116 Cather, S.M., Chapin, C.E., Kelley, S.A., 2012. Diachronous episodes of Cenozoic erosion in  
32  
33  
1117 southwestern North America and their relationship to surface uplift, paleoclimate,  
34  
35  
1118 paleodrainage, and paleoaltimetry. Geosphere 8 (6), 1177-1206.  
36  
37  
1119 <https://doi.org/10.1130/GES00801.1>  
38  
39  
40  
1120 Cermeño, P., Falkowski, P.G., Romero, O.E., Schaller, M.F., Vallina, S.M., 2015. Continental  
41  
42  
1121 erosion and the Cenozoic rise of marine diatoms. Proceedings National Academy of Sciences  
43  
44  
1122 U.S.A. 112 (14), 1–6. <https://doi.org/10.1073/pnas.1412883112>  
45  
46  
47  
1123 Churchill, M., Berta, A., Deméré, T., 2012. The systematic of right whales (Mysticeti: Balaenidae).  
48  
49  
1124 Mar. Mam. Sci. 28, 497–521.  
50  
51  
52  
1125 Collareta, A., Landini, W., Lambert, O., Post, K., Tinelli, C., Di Celma, C., Panetta, D., Tripodi,  
53  
54  
1126 M., Salvadori, P.A., Caramella, D., Marchi, D., Urbina, M., Bianucci, G., 2015. Piscivory in a  
55  
56  
1127 Miocene Cetotheriidae of Peru: first record of fossilized stomach content for an extinct baleen-  
57  
58  
1128 bearing whale. Sci. Nat. 102, 70.  
59  
60  
61  
62  
63  
64  
65



- 1129 Cortese, G., Gersonde, R., Hillenbrand, C.D., Kuhn, G., 2004a. Opal sedimentation shifts in and  
1 progression of the Messinian salinity crisis. *Nature* 400, 652–655. <http://doi.org/10.1038/23231>  
1130 2  
3  
4  
1131 Cortese, G., Gersonde, R., Hillenbrand, C.-D., Kuhn, G. 2004b. the World Ocean over the last 15  
5  
6  
1132 Ma. *Earth Planet. Sci. Lett.* 224, 509–527. <http://doi.org/10.1016/j.epsl.2004.05.035>  
7  
8  
9  
1133 Couvreur, T.L.P., Dauby, G., Blach-Overgaard, A., Deblauwe, V., Dessein, S., Droissart, V.,  
10  
11  
1134 Hardy, O.J., Harris, D.J., Janssens, S.B., Ley, A.C., Mackinder, B.A., Sonké, B., Sosef,  
12  
13  
1135 M.S.M., Stévar, T., Svenning, J.C., Wieringa, J.J., Faye, A., Missou, A.D., Tolley, K.A.,  
14  
15  
1136 Nicolas, V., Ntie, S., Fluteau, F., Robin, C., Guillocheau, F., Barboni, D., Sepulchre, P., 2020.  
16  
17  
1137 Tectonics, climate and the diversification of the tropical African terrestrial flora and fauna.  
18  
19  
20  
21  
1138 *Biological Reviews* 96 (1), 16-51. <https://doi.org/10.1111/brv.12644>  
22  
23  
24  
1139 D’Amato, M.E., Harkins, G.W., de Oliveira, T., Teske, P.R., Gibbons, M. J., 2008. Molecular  
25  
26  
1140 dating and biogeography of the neritic krill *Nyctiphanes*. *Mar. Biol.* 155, 243-247.  
27  
28  
1141 Damuth, J.D., MacFadden, B.J., 1990. *Body Size in Mammalian Paleobiology: Estimation and*  
29  
30  
1142 *Biological Implications*. Cambridge University Press, Cambridge  
31  
32  
33  
1143 Deméré, T.A., McGowen, M.R., Berta, A., Gatesy, J.. 2008. Morphological and molecular evidence  
34  
35  
1144 for a stepwise evolutionary transition from teeth to baleen in mysticete whales. *Syst. Biol.* 57,  
36  
37  
1145 15–37.  
38  
39  
40  
1146 Dickinson, J.A., Wallace, M.W., Holdgate, G.R., Gallagher, S.J., Thomas, L., 2002. Origin and  
41  
42  
1147 timing of the Miocene-Pliocene unconformity in Southeast Australia. *Journal of Sedimentary*  
43  
44  
1148 *Research* 72 (2), 288-303.  
45  
46  
47  
1149 Dominici, S., Danise, S., Cau, S., Freschi, A., 2020. The awkward distribution of fossil whales.  
48  
49  
50  
1150 *Earth-Science Reviews* 205, 103057.  
51  
52  
53  
1151 Døssing, A., Japsen, P., Watts, A.B., Nielsen, T., Jokat, W., Thybo, H., Dahl-Jensen, T., 2016.  
54  
55  
1152 Miocene uplift of the NE Greenland margin linked to plate tectonics: seismic evidence from the  
56  
57  
1153 Greenland Fracture Zone, NE Atlantic. *Tectonics* 35, 257-282.  
58  
59  
60  
1154 <https://doi.org/10.1002/2015TC004079>  
61  
62  
63  
64  
65

- 1155 Droser, M.L., 2003. Ecological changes through geological time. In: Briggs, D.E.G., Crowther, P.R.  
1  
1156 (Eds), Palaeobiology II. Blackwell Publishing, Malden, pp. 432–437  
2  
3  
4  
1157 Ekdale, E.G., Deméré, T.A., 2021. Neurovascular evidence for a co-occurrence of teeth and baleen  
5  
6  
1158 in an Oligocene mysticete and the transition to filter-feeding in baleen whales. Zool. J. Linn.  
7  
8  
1159 Soc. 194, 395–415.  
9  
10  
11  
1160 El Adli, J.J., Deméré, T.A., Boessenecker, R.W., 2014. *Herpetocetus morrowi* (Cetacea: Mysticeti),  
12  
13  
1161 a new species of diminutive baleen whale from the Upper Pliocene (Piacenzian) of California,  
14  
15  
1162 USA, with observations on the evolution and relationships of the Cetotheriidae. Zool. J. Linn.  
16  
17  
1163 Soc. 170, 400–466.  
18  
19  
20  
21  
1164 Elshaafi, A., Gudmundsoon, A., 2021. Central volcanoes and caldera collapses in the late Miocene-  
22  
23  
1165 Late Pleistocene Tibesti Volcanic Province, northwest Chad. Journal of Geodynamics 145,  
24  
25  
1166 101846. <https://doi.org/10.1016/j.jog.2021.101846>  
26  
27  
28  
1167 Figueiredo, J., Hoorn, C., van der Ven, P., Soares, E., 2009. Late Miocene onset of the Amazon  
29  
30  
1168 River and the Amazon deep-sea fan: evidence from the Foz do Amazonas Basin. Geology 37,  
31  
32  
1169 619-622. <https://doi.org/10.1130/G25567A.1>  
33  
34  
35  
1170 Filippelli, G.M., 1997. Intensification of the Asian monsoon and a chemical weathering event in the  
36  
37  
1171 late Miocene-early Pliocene: implications for the late Neogene climate change. Geology 25 (1),  
38  
39  
1172 27-30. [http://doi.org/10.1130/0091-7613\(1997\)025<0027:IOTAMA>2.3.CO;2](http://doi.org/10.1130/0091-7613(1997)025<0027:IOTAMA>2.3.CO;2)  
40  
41  
42  
1173 Fordyce, R.E., 1980. Whale evolution and Oligocene Southern Ocean environments. Palaeogeogr.  
43  
44  
1174 Palaeoecol. Palaeocl. 31, 319–336.  
45  
46  
47  
1175 Fordyce, R.E., 1977. The development of the circum-Antarctic current and the evolution of the  
48  
49  
1176 Mysticeti (Mammalia: Cetacea). Palaeogeogr. Palaeoecol. Palaeocl. 21,265–271.  
50  
51  
52  
1177 Fordyce, R.E., Marx, F.G., 2018. Gigantism precedes filter feeding in baleen whale evolution. Curr.  
53  
54  
1178 Biol. 28, 1670–1676.  
55  
56  
57  
58  
59  
60  
61  
62  
63  
64  
65

- 1179 Galloway, W.E., Witheaker, T.L., Ganey-Curry, P., 2011. History of Cenozoic North American  
1 drainage basin evolution, sediment yield, and accumulation in the Gulf of Mexico basin.  
1180  
2  
3  
4  
1181 Geology 7 (4), 938-973. <https://doi.org/10.1130/GES00647.1>  
5  
6
- 1182 Gatesy, J., Ekdale, E.G., Deméré, T.A., Lanzetti, A., Randall, J., Berta, A., El Adli, J., Springer,  
7  
8  
9  
1183 M.S., McGowen, M.R., 2022. Anatomical, ontogenetic, and genomic homologies guide  
10  
11  
1184 reconstructions of the teeth-to-baleen transition in mysticete whales. BioRxiv preprint doi:  
12  
13  
14  
1185 <https://doi.org/10.1101/2022.03.10.483660>  
15  
16
- 1186 Gavrilchuk, K., Lesage, V., Ramp, C., Sears, R., Bérubé, M., Bearhop, S., Beauplet, G., 2014.  
17  
18  
1187 Trophic niche partitioning among sympatric baleen whale species following the collapse of  
19  
20  
21  
1188 groundfish stocks in the Northwest Atlantic. *Mari. Ecol. Progr. Ser.* 497, 285–301.  
22  
23
- 1189 Geisler, J.H., McGowen, M.R., Yang, G., Gatesy, J., 2011. A supermatrix analysis of genomic,  
24  
25  
26  
1190 morphological, and paleontological data from crown Cetacea. *BMC Evol. Biol.* 11, 1–33.  
27  
28
- 1191 Gingerich, P.D., Uhen, M.D., 1998. Likelihood estimation of the time of origin of Cetacea and the  
29  
30  
31  
1192 time of divergence of Cetacea and Artiodactyla. *Palaeontol. Electronica*  
32  
33  
1193 <https://doi.org/10.26879/98008>  
34  
35
- 1194 Gladstone, R., Flecker, R., Valdes, P., Lunt, D., Marwick, P., 2007. The Mediterranean hydrologic  
36  
37  
38  
1195 budget from a Late Miocene global climate simulation. *Palaeogeography, Palaeoclimatology,*  
39  
40  
41  
1196 *Palaeoecology* 251, 254–267. <http://doi.org/10.1016/j.palaeo.2007.03.050>  
42  
43
- 1197 Goldbogen, J.A., Cade, D.E., Wisniewska, D.M., Potvin, J., Segre, P.S., Savoca, M.S., Hazen, E.L.,  
44  
45  
46  
1198 Czapanskiy, M.F., Kahane-Rapport, S.R., Deruiter, S.L., Gero, S., Tønnesen, P., Gough, W.T.,  
47  
48  
1199 Hanson, M.B., Holt, M.M., Jensen, F.H., Simon, M., Stimpert, A.K., Arranz, P., Johnston,  
49  
50  
51  
1200 D.W., Nowacek, D.P., Parks, S.E., Visser, F., Friedlaender, A.S., Tyack, P.L., Madsen, P.T.,  
52  
53  
1201 Pyenson, N.D., 2019. Why whales are big but not bigger: physiological drivers and ecological  
54  
55  
1202 limits in the age of ocean giants. *Science* 366, 1367–1372.  
56  
57
- 1203 Goloboff, P.A., Catalano, S.A., 2016. TNT version 1. 5, including a full implementation of  
58  
59  
60  
1204 phylogenetic morphometrics. *Cladistics* 32, 231–238.  
61  
62  
63  
64  
65

- 1205 Griffin, D.L., 2002. Aridity and humidity: two aspects of the late Miocene climate of North Africa  
1  
1206 and the Mediterranean. *Palaeogeography, Palaeoclimatology, Palaeoecology* 182, 65–91.  
2  
3  
4  
1207 Griffin, D.L., 2006. The late Neogene Sahabi rivers of the Sahara and their climatic and  
5  
6  
1208 environmental implications for the Chad Basin. *Journal of the Geological Society* 163, 905–  
7  
8  
9  
1209 921.  
10  
11  
1210 Guo, Z.T., Ruddiman, W.F., Hao, Q.Z., Wu, H.B., Qiao, Y.S., Zhu, R.X., Peng, S.Z., Wei, J.J.,  
12  
13  
14  
1211 Yuan, B.Y., Liu, T.S., 2002. Onset of Asian desertification by 22 Myr inferred from loess  
15  
16  
1212 deposits in China. *Nature* 416, 159-163. <https://doi.org/10.1038/416159a>  
17  
18  
19  
1213 Hammer, Ø., Harper, D.A.T., Ryan, P.D., 2001. PAST: paleontological statistics software package  
20  
21  
1214 for education and data analysis. *Palaeontol. Electronica* 4, 4.  
22  
23  
24  
1215 Haq, B.U., Hardenbol, J., Vail, P.R., 1987. Chronology of fluctuating sea levels since the Triassic.  
25  
26  
1216 *Science* 235, 1156–1167. <https://doi.org/10.1126/science.235.4793.1156>  
27  
28  
1217 [http://doi.org/10.1016/S0031-0182\(01\)00453-9](http://doi.org/10.1016/S0031-0182(01)00453-9)  
29  
30  
31  
1218 Hocking, D.P., Marx, F.G., Park, T., Fitzgerald, E.M.G., Evans, A.R., 2017. A behavioural  
32  
33  
1219 framework for the evolution of feeding in predatory aquatic mammals. *Proc. R. Soc. B* 284,  
34  
35  
1220 20162750. <http://dx.doi.org/10.1098/rspb.2016.2750>  
36  
37  
38  
1221 Huelsenbeck, J.P., 1994. Comparing the stratigraphic record to estimates of phylogeny.  
39  
40  
1222 *Paleobiology* 20, 470–483.  
41  
42  
43  
1223 Hyeong, K., Kim, J., Yoo, C.M., Moon, J.W., Seo, I., 2013. Cenozoic history of phosphogenesis  
44  
45  
1224 recorded in the ferromanganese crusts of central and western Pacific seamounts: implications  
46  
47  
1225 for deepwater circulation and phosphorus budgets. *Palaeogeography, Palaeoclimatology,*  
48  
49  
50  
1226 *Palaeoecology* 392, 293-301. <https://doi.org/10.1016/j.palaeo.2013.09.012>  
51  
52  
53  
1227 Jarman, S.N., Elliott, N.G., Nicol, S., McMinn, A., 2000. Molecular phylogenetics of circumglobal  
54  
55  
1228 *Euphausia* species (Euphausiacea: Crustacea). *Can. J. Fish. Aqu. Sci.* 57 (Suppl. 3). 51–58.  
56  
57  
58  
1229 Jordan, T.E., Kirk-Lawlor, N.E., Blanco, N., Rech, J.A., Cosentino, N.J., 2014. Landscape  
59  
60  
1230 modification in response to repeated onset of hyperarid paleoclimate states since 14 Ma,  
61  
62  
63  
64  
65

- 1231 Atacama Desert, Chile. Geological Society of America Bulletin 126 (7-8), 1016-1046.  
1  
1232 <https://doi.org/10.1130/B30978.1>  
3  
1233 Katz, O., 2019. Conflict and complementarity of paleontological and molecular chronologies?  
4  
6 Paleobiology 45, 7–20.  
734  
8  
9  
1235 Kawamura, A., 1980. A review of food of balaenopterid whales. Sci. Rep. Whales Res. Inst. 32,  
10  
11 155–197.  
1236  
13  
14  
1237 Keller, G., Barron, J.A., 1983. Paleooceanographic implications of Miocene deep-sea hiatuses.  
15  
16 Geological Society of America Bulletin 94, 590-613.  
1238  
18  
19  
1239 Kemp, A.E.S., Pearce, R.B., Grigorov, I., Rance, J., Lange, C.B., Quilty, P., Salter, I., 2006.  
20  
21 Production of giant marine diatoms and their export at oceanic frontal zones: implications for  
1240  
22 Si and C flux from stratified oceans. Global Biogeochemical Cycles 20 (4), 1-13.  
23  
24  
1241  
25 <https://doi.org/10.1029/2006GB002698>  
1242  
26  
27  
28  
1243 Kimura, T., 2002. Feeding strategy of an early Miocene cetother from the Toyama and Akeyo  
29  
30 Formations, central Japan. Palaeontol. Res. 6, 179–189.  
1244  
31  
32  
33  
1245 Kooistra, W.H.C.F., Gersonde, R., Medlin, L.K., Mann, D.G., 2007. The origin and evolution of the  
34  
35 diatoms: their adaptation to a planktonic existence. In: Evolution of Primary Producers in the  
1246  
36 Sea (P.G. Falkowski, A.H. Knoll), Academic Press, pp. 207-249.  
1247  
37  
38  
39  
40  
1248 Kouwenhoven, T.J., van der Zwaan, G.J., 2006. A reconstruction of late Miocene Mediterranean  
41  
42 circulation patterns using benthic foraminifera. Palaeogeography, Palaeoclimatology,  
1249  
43  
44 Palaeoecology 238 (1), 373–385. <http://doi.org/10.1016/j.palaeo.2006.03.035>  
1250  
45  
46  
47  
48  
1251 Krijgsman, W., Hilgen, F.J., Raffi, I., Sierro, F.J., Wilson, D.S., 1999a. Chronology, causes  
49  
50  
1252 Maddison, W., Maddison, D., 2019. Mesquite 3.61: a modular system for evolutionary analysis.  
51  
52 Available at: <https://www.mesquiteproject.org/>  
1253  
53  
54  
55  
1254 Marx, F.G., Buono, M.R., Evans, A.R., Fordyce, R.E., Reguero, M., Hocking, D.P., 2019a.  
56  
57  
1255 Gigantic mysticete predators roamed the Eocene Southern Oceans. Antarct. Sci. 31, 98–104.  
58  
59  
60  
61  
62  
63  
64  
65

- 1256 Marx, F.G., Fordyce, R.E., 2015. Baleen boom and bust: a synthesis of mysticete phylogeny,  
1  
1257 diversity and disparity. Roy. Soc. Open Sci. 2, 140434.  
2  
3  
4  
1258 Marx, F.G., Fitzgerald, E.M.G., Fordyce, R.E., 2019b. Like phoenix from the ashes: how modern  
5  
6  
1259 baleen whales arose from a fossil “dark age”. Acta Palaeontol. Pol. 64, 231–238.  
7  
8  
9  
1260 Marx, F.D., Hocking, D., Park, T., Ziegler, T., Evans, A.R., Fitzgerald, E.M.G., 2016. Suction  
10  
11  
1261 feeding preceded filtering in baleen whale evolution. Memoirs of Museum Victoria 75:71-81.  
12  
13  
14  
1262 Marx, F.G., Uhen, M.D., 2010. Climate, critters, and cetaceans: Cenozoic drivers of the evolution  
15  
16  
1263 of modern whales. Science 327, 993–996.  
17  
18  
19  
1264 Matzke, N.J., Irmis, R.B., 2016. Including autapomorphies is important for paleontological tip-  
20  
21  
1265 dating with clocklike data, but not with non-clock data. PeerJ 6:e4553; DOI 10.7717/peerj.4553  
22  
23  
24  
1266 McGowen, M.R., Spaulding, M., Gatesy, J., 2009. Divergence date estimation and a comprehensive  
25  
26  
1267 molecular tree of extant cetaceans. Mol. Phyl. Evol. 53, 891–506.  
27  
28  
29  
1268 Mouthereau, F., 2011. Timing of uplift in the Zagros belt/Iranian plateau and accommodation of  
30  
31  
1269 late Cenozoic Arabia-Eurasia convergence. Geological Magazine 148 (5-6), 726-738.  
32  
33  
1270 <https://doi.org/10.1017/S0016756811000306>  
34  
35  
36  
1271 Muizon, C. de, Bianucci, G., Martínez-Cáceres, M., Lambert, O., 2019. *Mystacodon selenensis*, the  
37  
38  
1272 earliest known toothed mysticete (Cetacea, Mammalia) from the late Eocene of Peru: anatomy,  
39  
40  
1273 phylogeny, and feeding adaptations. Geodiversitas 41, 401–499.  
41  
42  
43  
1274 Ollier, C.D., Pain, C.F., 2019. Neotectonic mountain uplift and geomorphology. Geomorfologiya 4,  
44  
45  
1275 3-26. <https://doi.org/10.31857/S0435-4281201943-26>  
46  
47  
48  
1276 O’Leary, M., Uhen, M.D., 1999. The time of origin of whales and the role of behavioral changes in  
49  
50  
1277 the terrestrial-aquatic transition. Paleobiology 25, 534–556.  
51  
52  
53  
1278 Pellegrino, L., Dela Pierre, F., Natalicchio, M., Carnevale, G., 2018. The Messinian diatomite  
54  
55  
1279 deposition in the Mediterranean and its relationships to the global silica cycle. Earth-Science  
56  
57  
1280 Reviews 178, 154-176. <https://doi.org/10.1016/j.earscirev.2018.01.018>  
58  
59  
60  
61  
62  
63  
64  
65

- 1281 Peredo, C.M., Pyenson, N.D., Boersma, A.T., 2017. Decoupling tooth loss from the evolution of  
1  
2  
1282 baleen in whales. *Front. Mar. Sci.* 4, 67. doi: 10.3389/fmars.2017.00067  
3  
4  
1283 Peredo, C.M., Pyenson, N.D., Uhen, M.D., 2022. Lateral palatal foramina do not indicate baleen in  
5  
6  
1284 fossil whales. *Sci. Rep.*, 11448.  
7  
8  
1285 Pérez-Escobar, O.A., Zizka, A., Bermúdez, M.A., Meseguer, A.S., Condamine, F.L., Hoorn, C.,  
9  
10  
1286 Hooghiemstra, H., Pu, Y., Bogarín, D., Boschman, L.M., Pennington, R.T., Antonelli, A.,  
11  
12  
1287 Chomicki, G., 2022. The Andes through time: evolution and distribution of Andean floras.  
13  
14  
1288 *Trends in Plant Science* 27 (4), 364-378. <https://doi.org/10.1016/j.tplants.2021.09.010>  
15  
16  
1289 Pershing, A.J., Christensen, L.B., Record, N.R., Sherwood, G.D., Stetson, P.B., 2010. The impact  
17  
18  
1290 of whaling on the ocean carbon cycle: why bigger was better. *PLoS ONE* 5, e12444.  
19  
20  
1291 Pershing, A.J., Stamieszkin, K., 2020. The North Atlantic ecosystem, from plankton to whales.  
21  
22  
1292 *Annu. Rev. Mar. Sci.* 12, 339–359.  
23  
24  
1293 Potter, P.E., Sztamari, P., 2009. Global Miocene tectonics and the modern world. *Earth-Science*  
25  
26  
1294 *Reviews* 96, 279-295. <https://doi.org/10.1016/j.earscirev.2009.07.003>  
27  
28  
1295 Potter, P.E., Sztamari, P., 2015. The global Middle and Late Miocene and the deep earth: model for  
29  
30  
1296 earlier orogenies. *Marine and Petroleum Geology* 68, 178–191.  
31  
32  
1297 <https://doi.org/10.1016/j.marpetgeo.2015.08.021>  
33  
34  
1298 Pyenson, N.D., Sponberg, S.N., 2011. Reconstructing body size in extinct crown cetacea (Neoceti)  
35  
36  
1299 using allometry, phylogenetic methods and tests from the fossil record. *J. Mam. Evol.* 18, 269–  
37  
38  
1300 289.  
39  
40  
1301 Rea, D.K., 1992. Delivery of Himalayan sediment to the northern Indian Ocean and its relation to  
41  
42  
1302 global climate sea level, uplift, and seawater strontium. In: Duncan, R.A., Rea, D.K., Kidd,  
43  
44  
1303 R.B., von Rad, U., Weissel, J.K., (Eds.), *Synthesis of Results from Scientific Drilling in the*  
45  
46  
1304 *Indian Ocean. Geophysical Monograph* 70, American Geophysical Union, 387-402.  
47  
48  
1305 Renaudie, J., 2016. Quantifying the Cenozoic marine diatom deposition history: links to the C and  
49  
50  
1306 Si cycles. *Biogeosciences* 13, 6003-6014. <https://doi.org/10.5194/bg-13-6003-2016>  
51  
52  
53  
54  
55  
56  
57  
58  
59  
60  
61  
62  
63  
64  
65

- 1307 Rivadeneira, M., Hunt, G., Roy K., 2009. The use of sighting records to infer species extinctions: an  
1  
1308 evaluation of different methods. *Ecol.* 90, 1291–1300.  
2  
3  
4  
1309 Rognon, P., Gourinard, Y., Bandet, Y., Koeniguer, J.C., Delteil-Desneux F., 1983. Précisions  
5  
6  
1310 chronologiques sur l'évolution volcano-tectonique et géomorphologiques de l'Atakor (Hoggar):  
7  
8  
1311 apports des données radiométriques (K/Ar) et paléobotaniques (bois fossiles). *Bulletin Société*  
9  
10  
1312 *Géologique France* 25, 973-980.  
11  
12  
13  
14  
1313 Rohling, E.J., Marino, G., Grant, K.M., 2015. Mediterranean climate and oceanography, and the  
15  
16  
1314 periodic development of anoxic events (sapropels). *Earth-Science Reviews* 143, 62-97.  
17  
18  
1315 <https://doi.org/10.1016/j.earscirev.2015.01.008>  
19  
20  
21  
1316 Roman, J., Palumbi, S.R., 2003. Whales before whaling in the North Atlantic. *Science* 301, 508–  
22  
23  
1317 510.  
24  
25  
26  
1318 Rooney, A., Honeycutt, R.L., Derr, J.N., 2001. Historical population size change of bowhead  
27  
28  
1319 whales inferred from DNA sequence polymorphism data. *Evolution* 55, 1678–1685.  
29  
30  
31  
1320 Ryan, C., McHugh, B., Trueman, C.N., Sabin, R. et al., 2013 Stable isotope analysis of baleen  
32  
33  
1321 reveals resource partitioning among sympatric rorquals and population structure in fin whales.  
34  
35  
1322 *Mar. Ecol. Prog. Ser.* 479, 251–261.  
36  
37  
38  
1323 Sanderson, L.R., Wassersug, R., 1993. Convergent and alternative designs for vertebrate suspension  
39  
40  
1324 feeding. In: Hanken, J., Hall, B.K. (Eds.), *The skull: functional and evolutionary mechanisms*  
41  
42  
1325 (volume 3). University Press of Chicago, Chicago, pp. 37–112.  
43  
44  
45  
1326 Santini, F., Carnevale, G., 2015. First multilocus and densely sampled timetree of trevallies,  
46  
47  
1327 pompanos and allies (Carangoidei, Percomorpha) suggests a Cretaceous origin and Eocene  
48  
49  
1328 radiation of a major clade of piscivores. *Molecular Phylogenetics and Evolution* 83, 33-39.  
50  
51  
52  
1329 Santini, F., Carnevale, G., Sorenson, L., 2013. First molecular scombrid timetree (Scombridae,  
53  
54  
1330 Percomorpha) shows recent radiation of tunas following invasion of pelagic habitats. *Italian*  
55  
56  
1331 *Journal of Zoology* 80, 210-221.  
57  
58  
59  
60  
61  
62  
63  
64  
65



- 1332 Sarkar, S., Basak, C., Frank, M., Berndt, C., Huuse, M., Badhani, S., Bialas, J., 2019. Late Eocene  
1  
1333 onset of the Proto-Antarctic Circumpolar Current. *Scientific Reports* 9 (10125), 1-10.  
2  
3  
4  
1334 <https://doi.org/10.1038/s41598-019-46253-1>  
5  
6
- 1335 Sasaki, T., Nikaido, M., Hamilton, H., Goto, M., Kato, H., Kanda, N., Pastene, L.A., Cao, Y.,  
7  
8  
9  
1336 Fordyce, R.E., Hasegawa, M., Okada, N., 2005. Mitochondrial phylogenetics and evolution of  
10  
11  
1337 mysticete whales. *Syst. Biol.* 54, 77–90.  
12  
13
- 1338 Savoca, M.S., Czapanskiy, M.F., Kahane-Rapport, S.R., Gough, W.T., Fahlbusch, J.A., Bierlich,  
14  
15  
16  
1339 K.C., Segre, P.S., Di Clemente, J., Penry, G.S., Wiley, D.N., Calambokidis, J., Nowacek, D.P.,  
17  
18  
19  
1340 Johnston, D.W., Pyenson, N.D., Friedlaender, A.S., Hazen, E.L., Goldbogen, J.A., 2021.  
20  
21  
1341 Baleen whale prey consumption based on high-resolution foraging measurements. *Nature* 599,  
22  
23  
1342 85–90.  
24  
25
- 1343 Schuster, M., Düringer, P., Ghienne, J.F., Vignaud, P., Mackaye, H.T., Likius, A., Brunet, M.,  
26  
27  
28  
1344 2006. The age of the Sahara Desert. *Science* 311, 821. <https://doi.org/10.1126/science.1120161>  
29  
30
- 1345 Schwarzhan, W., Carnevale, G., 2021. The rise to dominance of lanternfishes (Teleostei:  
31  
32  
33  
1346 Myctophidae) in the oceanic ecosystems: a paleontological perspective. *Paleobiology* 47 (3),  
34  
35  
1347 446-463. <https://doi.org/10.1017/pab.2021.2>  
36  
37
- 1348 Scotese, C.R., Song, H., Mills, B.J.W., van der Meer, D.G., 2021. Phanerozoic paleotemperatures:  
38  
39  
40  
1349 the Earth's changing climate during the last 540 million years. *Earth-Science Reviews* 215,  
41  
42  
43  
1350 103503. <https://doi.org/10.1016/j.earscirev.2021.103503>  
44  
45
- 1351 Senut, B., Pickford, M., Ségalen, L., 2009. Neogene desertification of Africa. *Comptes Rendus*  
46  
47  
48  
1352 *Geoscience* 341, 591-602. <https://doi.org/10.1016/j.crte.2009.03.008>  
49  
50
- 1353 Sepkoski, J.J. Jr, 1981. A factor analytic description of the Phanerozoic marine fossil record.  
51  
52  
1354 *Paleobiology* 7, 36–53.  
53  
54
- 1355 Sepulchre, P., Ramstein, G., Fluteau, F., Schuster, M., Tiercelin, J.J., Brunet, M.J., 2006. Tectonic  
55  
56  
57  
1356 uplift and Eastern Africa aridification. *Science* 313 (5792), 1419-1423.  
58  
59  
1357 <http://doi.org/10.1126/science.1129158>  
60  
61

- 1358 Slater, G.J., Goldbogen, J.A., Pyenson, N.D., 2017. Independent evolution of baleen whale  
1  
1359 gigantism linked to Plio-Pleistocene ocean dynamics. *Proc. Roy. Soc. B* 284, 20170546.  
3  
4  
1360 Smith, T.J., Puttick, M.N., O'Reilly, J.E., Pisani, D., Donoghue, P.C.J., 2021. Phylogenetic  
6  
1361 sampling affects evolutionary patterns of morphological disparity. *Palaeontology* 64, 765-787.  
8  
9  
1362 Soltis, P.S., Soltis, D.E., 2003. Applying the bootstrap in phylogeny reconstruction. *Stat. Sci.* 18,  
10  
1363 256-267.  
13  
14  
1364 Steeman, M.E., Hebsgaard, M.B., Fordyce, R.E., Ho, S.Y.W., Rabosky, D.L., Nielsen, R., Rahbek,  
15  
16 C., Glenner, H., Sørensen, M., Willerslev, E., 2009. Radiation of extant cetaceans driven by  
18  
1365 restructuring of the oceans. *Syst. Biol.* 58,573–585.  
19  
20  
21  
1366 Steinhorsdottir, M., Coxall, H.K., de Boer, A.M., Huber, M., Barbolini, N., Bradshaw, C.D., Burls,  
23  
24 N.J., Feakins, S.J., Gasson, E., Henderiks, J., Holbourn, A.E., Kiel, S., Kohn, M.J., Knorr, G.,  
25  
26 Kürschner, W.M., Lear, C.H., Liebrand, D., Lunt, D.J., Mörs, T., Pearson, P.N., Pound, M.J.,  
27  
28 Stoll, H., Strömberg, C.A.E., 2021. The Miocene: the Future of the Past. *Paleoceanography and*  
29  
30  
1371 *Paleoclimatology* 36, e2020PA004037. <https://doi.org/10.1029/2020PA004037>  
32  
33  
1372 Sternai, P., Caricchi, L., Pasquero, C., Garzanti, E., van Hinsbergen, D.J.J., Castelltort, S., 2019.  
35  
1373 Magmatic forcing of Cenozoic climate? *Journal of Geophysical Research: Solid Earth* 125,  
36  
37 e2018JB016460. <https://doi.org/10.1029/2018JB016460>  
38  
39  
40  
1374  
41  
1375 Strauss, D., Sadler, P.M. 1989. Classical confidence intervals and Bayesian probability estimates  
42  
43 for ends of local taxon ranges. *Math. Geol.* 21, 411–427.  
44  
45  
1376  
46  
1377 Strömberg, C.A.E., Staver, A.C., 2022. The history and challenge of grassy biomes. *Science* 377  
47  
48 (6606), 592-593. <https://doi.org/10.1126/science.add1347>  
49  
50  
1379 Suto, I., 2006. The explosive diversification of the diatom genus *Chaetoceros* across the  
52  
53 Eocene/Oligocene and Oligocene/Miocene boundaries in the Norwegian Sea. *Marine*  
54  
55 *Micropaleontology* 58, 259-269. <https://doi.org/10.1016/j.marmicro.2005.11.004>  
56  
57  
1380  
58  
1382 Tsai, C.-H., Ando, T., 2016. Niche partitioning in Oligocene toothed mysticetes (Mysticeti:  
59  
60 Aetiocetidae). *J. Mam. Evol.* 23, 33–41.  
61  
62  
63  
64  
65

1384 Tsai, C.-H., Kohno, N., 2016. Multiple origins of gigantism in stem baleen whales. *Sci. Nat.* 103,  
1 89 10.1007/s00114-016-1417-5

1385  
2  
3  
4  
1386 Vidal, V., Bonneville, A., 2004. Variations of the Hawaiian hot spot activity revealed by variations  
5 in the magma production rate. *Journal of Geophysical Research* 109, B03104.  
6  
7  
8  
9  
10  
11  
12  
1387  
1388 <https://doi.org/10.1029/2003JB002559>

1389 Wang, S.C., Marshall, C.R., 2016. Estimating times of extinction in the fossil record. *Biol. Lett.*  
13 122015098920150989. <http://doi.org/10.1098/rsbl.2015.0989>

1390  
14  
15  
16  
1391 Whitmore, F.C. Jr., 1994. Neogene climatic change and the emergence of the modern whale fauna  
18 of the North Atlantic Ocean. In: Berta, A., Deméré, T.A. (Eds.), *Contributions in marine*  
19  
20  
21  
22  
23  
24  
25  
26  
27  
28  
29  
30  
31  
32  
33  
34  
35  
36  
37  
38  
39  
40  
41  
42  
43  
44  
45  
46  
47  
48  
49  
50  
51  
52  
53  
54  
55  
56  
57  
58  
59  
60  
61  
62  
63  
64  
65

1408 **Captions to illustrations**

1409 **Figure 1.** Stratigraphic distributions of mysticete species based on data downloaded from the  
1  
1410 Paleobiology Database. Main mysticete groups are indicated. The thick lines correspond to FAD  
2  
1411 and LAD for species represented by more than one specimen, and, for species represented by the  
3  
4  
5  
6  
1412 holotype only, to the errors of the estimations of the geological age of such a specimen. Scale  
7  
8  
9  
1413 generated through TSCreator visualization of enhanced Geologic Time Scale 2016 database  
10  
11  
1414 (Version 7.4; 2022), James Ogg (database coordinator)  
12  
13  
1415 <https://engineering.purdue.edu/Stratigraphy/tscreator>.  
14  
15  
16

1416  
17  
18  
19 **Figure 2.** Strict consensus (Nelsen) cladogram resulting from the present paper with indication of  
20  
21 bootstrap (bold numbers) and symmetric resampling (regular numbers) supporting values, and main  
22  
1418 mysticete clades.  
23  
24  
25  
26

1420  
27  
28  
29 **Figure 3.** Phylogenetic relationships of mysticete family-rank clades obtained by collapsing internal  
30  
31 nodes of monophyletic groups shown in Figure 2. Main mysticete suprafamily clades are indicated.  
32  
33

1423  
34  
35  
36 **Figure 4.** Phylogenetic relationships of family- and suprafamily-rank mysticete clades plotted  
37  
38 against a temporal scale showing the stratigraphic distributions of the groups and main  
39  
40 diversification events in yellow ellipses. In this plot, the thick lines are drawn based on all the  
1426  
41  
42 available data including FAD and LAD of species represented by more than one specimen, and the  
1427  
43  
44 error in the estimation of the geological age of the holotype in species represented by only one  
45  
1428  
46  
47 specimen.  
48  
1429  
49  
50

1430  
51  
52  
53 **Figure 5.** Plots illustrating the changes in diversity occurred throughout mysticete evolutionary  
54  
55 history against a temporal scale. A, alpha diversity based on fossil and extant species occurrences.  
1432  
56  
57 B, clade diversity. The main diversification events are indicated by Greek letters.  
58  
1433  
59  
60

1434  
61  
62  
63  
64  
65

1435 **Figure 6.** Patterns of extinction and origination throughout the mysticete evolution. **a**, alpha  
1  
1436 origination rates per million years. **b**, clade origination rates per million years. **c**, alpha extinction  
2  
1437 rates per million years. **d**, clade extinction rates per million year.  
3  
4  
5  
6

7  
1438  
8  
1439 **Figure 7.** Phylogenetic relationships of mysticetes plotted against a temporal scale with indication  
9  
1440 of main mysticete clade. Phylogenetic relationships are from cladogram in Figure 3 and analysis  
10  
1441 from present paper. Thin lines represent ghost lineages. Thick lines represent all the available  
11  
1442 information about the stratigraphic distributions of the species: FAD and LAD for species  
12  
1443 represented by more than one specimen, and error in the estimation of the geological ages of the  
13  
1444 holotypes for species represented by one specimen only. Note that the times of origin of main  
14  
1445 clades (at internal nodes) are those reported in Table 1.  
15  
16  
17  
18  
19  
20  
21  
22  
23

24  
25  
1446  
26  
27  
28  
29  
1447 **Figure 8.** ‘Evolutionray faunas’. Plots comparing occurrences and clade numbers of different  
30  
1448 mysticete family-rank clades against a temporal scale showing diversity trends and eventual  
31  
1449 competition dynamics. Greek and Latin letters between the two plots represent major diversification  
32  
33  
1450 events presented in Figure 4.  
34  
35  
36  
37  
38

39  
40  
1451  
41  
1452 **Figure 9.** Rates of morphological changes at particular transition events throughout mysticete  
42  
1453 evolution.  
43  
44  
45

46  
1454  
47  
48  
1455 **Figure 10.** Box plot showing body size change throughout mysticete evolution. White circles  
49  
50  
1456 correspond to outliers.  
51  
52

53  
1457  
54  
55  
1458 **Figure 11.** Ancestral state reconstruction and evolution of body size in mysticetes. Blue  
56  
57  
1459 corresponds to small size (total length < 8 m); yellow corresponds to middle size (total length  
58  
59  
1460 included between 9 and 13 m); orange corresponds to large size (total length included between 14  
60  
61  
62  
63  
64  
65

1461 and 20 m); red corresponds to gigantic size (total length > 20 m). Thick lines represent stratigraphic  
1  
1462 distributions of species generated by taking in mind all the available information including FAD  
3  
1463 and LAD for species represented by more than one specimen, and error in the estimation of the  
4  
6  
1464 geological ages of the holotypes for species represented by one specimen only.  
8

1465  
11  
1466 **Figure 12.** Mysticete body size and clade diversity compared to: CO<sub>2</sub> concentration – Renaudie  
13  
1467 (2016); global average temperature (LOWI: Late Oligocene Warm Interval; EMCI: Early Miocene  
14  
15  
1468 Cool Interval; MMTM: Middle Miocene Thermal Maximum; LMCI: Late Miocene Cool Interval;  
16  
18  
1469 MG: Messinian Glaciations; PTM: Pliocene Thermal Maximum; LGM: Last Glacial Maximum;  
20  
21  
1470 PIA: Pleistocene Ice Age) – Scotese et al. (2021); ice-sheet evolution – Zachos et al. (2001); sea  
22  
23  
1471 level – Haq et al. (1987); carbon isotopes – Zachos et al. (2001); diatom abundance and diversity –  
24  
25  
1472 Renaudie (2016); strontium isotopes – Renaudie (2016); sediment yield – Sternai et al. (2021);  
26  
27  
1473 detrital contribution vs. eolian quartz – Zheng (2016); dissolved silicon flux – Cermeño et al.  
28  
30  
1474 (2015).  
31  
32

33  
1475  
35  
1476 **Figure 13.** Mysticete body size and clade diversity compared to: terrestrial ecosystems evolution  
36  
37  
1477 comprising grasslands (1: first open-habitat grass in North America; 2: first grass-dominated habitat  
38  
39  
1478 in North America; 3: first grass-dominated habitat in Africa; 4: first open-habitat grass in Australia;  
40  
41  
1479 5: first grass-dominated habitat in Australia) – Strömberg & Staver (2022), grazers (1: first common  
42  
43  
1480 in North America; 2: first common in Africa; 3: first common in Australia) – Strömberg & Staver  
44  
45  
1481 (2022), fires (1: increase in Australia; 2: increase in Africa) – Strömberg & Staver (2022) and  
46  
47  
1482 deserts (1: onset of Asian desertification – Guo et al., 2002; 2: onset of Namib desert – Senut et al.,  
48  
49  
1483 2009; 3: onset of Atacama desert – Jordan et al., 2014; 4: onset of Sahara desert – Schuster et al.,  
50  
51  
1484 2006); global rates of ridge spreading – Potter and Szatmari (2009); main tectonic and volcanic  
52  
53  
1485 events occurred in Africa (Red Sea rifting – Boone et al., 2021; Hoggar volcanism – Rognon et al.,  
54  
55  
1486 1983; Aït-Hamou et al., 2000; Tibesti volcanic province – Elshaafi & Gudmundsson, 2021; onset of  
56  
57  
58  
59  
60  
61  
62  
63  
64  
65

1487 modern Congo river drainage, Ethiopian traps, Southern African Escarpment, uplift of Central  
 1  
 1488 African Atlantic Swell, East African Rift System – Couvreur et al., 2020; acceleration of East  
 2  
 1489 African Plateau – Sepulchre et al., 2006); Americas (Basin and Range volcanism – Sternai et al.,  
 3  
 2021; Columbia River flood basalt – Steinhorsdottir et al., 2021; Yellowstone Hotspots – Potter &  
 4  
 1490 Szatmari, 2015; Southwestern N. America uplift – Cather et al., 2012; Great Basin Ignimbrites –  
 5  
 1491 Sternai et al., 2021; Southern Cordillera uplift – Cather et al., 2012; Andean orogeny, acceleration  
 6  
 1492 of Andean uplift – Pérez-Escobar et al., 2022; Drake Passage opening, Panama Isthmus shoaling –  
 7  
 1493 Potter and Szatmari, 2015; Amazon Fan sedimentation rate – Figueiredo et al., 2009; Gulf of  
 8  
 1494 Mexico clastic deposition – Galloway et al., 2011; Eurasia (Bengal and Nicobar Fan sedimentation  
 9  
 1495 rate – Betka et al., 2021; Tethys closure – Potter & Szatmari, 2015; enhanced erosion of Alps –  
 10  
 1496 Willett, 2010; Greenland-Scotland Ridge opening – Potter & Szatmari, 2015; Himalayan orogeny -  
 11  
 1497 Cermeño et al., 2015; Tibetan-Plateau uplift increase, Greenland-Scotland Ridge opening – Potter  
 12  
 1498 & Szatmari, 2015; further acceleration of Himalaya uplift – Filippelli, 1997; N. Indian Ocean  
 13  
 1499 sediment influx – Rea, 1992; Mediterranean-Atlantic gateways closure – Kouwenhoven & van der  
 14  
 1500 Zwaan, 2006; strong increase of riverine runoff in the Mediterranean – Griffin, 2002, 2006,  
 15  
 1501 Gladstone et al., 2007; increase of circum-Mediterranean volcanism, Burma Basin, Mekong River,  
 16  
 1502 Red River, South China Margin, East China Margin clastic deposition – Potter and Szatmari, 2015;  
 17  
 1503 Hawaiian magma flux – Vidal & Bonneville, 2004; Zagros uplift increase – Mouthereau, 2011;  
 18  
 1504 Iceland Plume volume flux – Døssing et al., 2016; Oceania (Development of New Zealand Alpine  
 19  
 1505 Fault, Tasmania-Antarctic Passage opening, Indonesian gateways closure - Potter & Szatmari,  
 20  
 1506 2009, 2015; tectonic activity in SE Australian basins, uplift of Papua New Guinea – Dickinson et  
 21  
 1507 al., 2002).  
 22  
 1508  
 23  
 1509  
 24  
 1510 **Figure 14.** Mysticete body size and ‘evolutionary faunas’ compared to oceanographic events and  
 25  
 1511 ecological turnovers in marine environment comprising: major phosphogenetic episodes – Hyeong  
 26  
 1512 et al. (2013); radiation of deep dwelling planktic foraminifera (Boscolo-Galazzo et al., 2022);  
 27

1513 increase of high productivity-adapted benthic foraminifera (Steinhorsdottir et al., 2021); low-to-  
1  
1514 mid latitude diatom decline, Indian Ocean diatom increase – Renaudie (2016); full establishment of  
2  
3  
4  
1515 Southern Ocean opal belt – Renaudie (2016); Oligocene-Miocene Carbon Maximum –  
5  
6  
1516 Steinhorsdottir et al. (2021); Atlantic to Pacific silica switch (uncertainties about the onset are  
7  
8  
9  
1517 indicated by question marks) – Keller & Barron, (1983), Barron (2022); Late Miocene Carbon  
10  
11  
1518 Isotope Shift, Monterey Event – Steinhorsdottir et al. (2021); opal deposition in S. Pacific – Sarkar  
12  
13  
14  
1519 (2019); Monterey event – Steinhorsdottir et al. (2021); Messinian Salinity Crisis – Krijgsman et al.  
15  
16  
1520 (1999); explosive *Chaetoceros* resting spore diversification and abundance in N. Atlantic, further  
17  
18  
19  
1521 *Chaetoceros* spore diversification in N. Atlantic and *Chaetoceros* spore drop in N. Atlantic – Suto  
20  
21  
22  
1522 (2006); Carbonate Crash, Late Miocene-Early Pliocene Biogenic Bloom – Steinhorsdottir et al.  
23  
24  
25  
1523 (2021); 1<sup>st</sup> significant opal deposition in Southern Ocean – Renaudie (2016); giant diatom ooze  
26  
27  
28  
1524 deposition in the oceans – Kemp et al. (2006); onset of coastal mid-latitude upwelling – Renaudie  
29  
30  
31  
1525 (2016); cyclical sapropelitic deposition in the Mediterranean – Rohling et al. (2015); NCW/NADW,  
32  
33  
34  
1526 AACC – Sarkar et al. (2019), Steinhorsdottir et al. (2021); Euphasiaceae evolution (1: divergence  
35  
36  
37  
1527 of *Nyctiphanes* clade; 2: common ancestor of *Nyctiphanes* species; 3: most recent common ancestor  
38  
39  
40  
1528 of *Nyctiphanes australis*, *N. capensis* and *N. couchii*; 4: most recent common ancestor of *N.*  
41  
42  
43  
1529 *australis* and *N. capensis*) – D’Amato et al. (2008); Diaphinae evolution – Schwarzhans &  
44  
45  
46  
47  
48  
49  
50  
51  
52  
53  
54  
55  
56  
57  
58  
59  
60  
61  
62  
63  
64  
65